nature communications

Article

https://doi.org/10.1038/s41467-025-68220-3

O-GlcNAcylation of AMFR stabilizes TSPAN4 to regulate migrasome formation for viral release

Received: 10 February 2025

Accepted: 23 December 2025

Published online: 07 January 2026

Check for updates

Linghui Yu[1,2,6], Jiajia Li[2,3,6], Yiyang Han[4,6], Xiao Yang[2,3], Yu Fu[2], Weiyi Zhang[2], Yaming Jiu[5], Linling Cheng[2,3] ✉ & Binbin Ding[2,3] ✉

Migrasomes are migration-dependent organelles, serving as delivery packets to mediate release of cytoplasmic contents. Tetraspanin 4 (TSPAN4) acts as a marker for migrasomes and is essential for their formation. However, the regulatory mechanism(s) underlying TSPAN4-mediated migrasome biogenesis and its physiological functions remain to be elucidated. Here, we identified AMFR, an ER-resident E3 ligase, regulates migrasome formation through catalyzing the K48-linked polyubiquitination of TSPAN4 for degradation. Further, *O*-GlcNAcylation of AMFR by OGT at threonine 643 disrupts AMFR-TSPAN4 interactions, thereby stabilizing TSPAN4 and promoting migrasome formation. Additionally, viruses dynamically regulate migrasome formation by modulating AMFR *O*-GlcNAcylation and TSPAN4 ubiquitination. During the early stages of VSV or HSV-1 infection, viruses enhance migrasome formation and exploit these structures to spread among neighboring cells, whereas abolish migrasome formation during the late stages of infection. Our findings reveal a negatively regulatory mechanism governing migrasome biogenesis, and highlight how VSV and HSV-1 manipulate this process to facilitate their release.

Migrasomes are newly discovered organelles in migrating cells that mediating release of cytoplasmic contents, including mRNA, proteins, and mitochondria[1–3]. When cells migrate on extracellular substrates, retraction fibers (RFs) are pulled out of the plasma membrane and then migrasomes subsequently form on the RFs, and are left behind when cells migrate away and the RFs break. The discarded migrasomes can be taken up by surrounding cells, facilitating cell-to-cell communication[2]. Recent studies have demonstrated that migrasomes play important roles in organ morphogenesis and angiogenesis during embryonic development[4,5]. Additionally, migrasomes also contribute to various pathological conditions, including ischemic brain damage, proliferative vitreoretinopathy, cerebral amyloid angiopathy[6–8]. As one of the extracellular vesicles, migrasomes are found to play a role in virus replication[9–12]. But the molecular mechanisms remain largely unknown.

Tetraspanin 4 (TSPAN4) was previously found to be abundant in the migrasome membrane and act as a marker for migrasomes[13]. TSPAN4 belongs to the tetraspanin family, which has 33 members and all contain four transmembrane domains and are found in every cell type[14]. Tetraspanin family can separate in the membrane plane into tetraspanin-enriched microdomains[15]. Using live-cell system in vivo and reconstituted membrane system in vitro, recent study proposes that TSPAN4, together with cholesterol, are necessary and sufficient for migrasome formation[16]. During migrasome formation, TSPAN4 was

[1]Department of Biochemistry and Molecular Biology, School of Basic Medicine, Huazhong University of Science and Technology, Wuhan, China. [2]Guangzhou National Laboratory, Guangzhou, China. [3]State Key Laboratory of Respiratory Disease, National Clinical Research Center for Respiratory Disease, Guangzhou Institute of Respiratory Health, the First Affiliated Hospital of Guangzhou Medical University, Guangzhou, China. [4]The Division of Biology and Biological Engineering, California Institute of Technology, Pasadena, CA, USA. [5]Shanghai Institute of Materia Medica, Chinese Academy of Sciences, Shanghai, China. [6]These authors contributed equally: Linghui Yu, Jiajia Li, Yiyang Han. ✉e-mail: linling@gird.cn; dingbinbin1988@163.com

dynamically recruited to migrasomes and form discrete fast-moving puncta that concentrate on the migrasome membrane[16]. Notably, overexpression of TSPAN4 can induce migrasome formation, while depletion of TSPAN4 impairs migrasome formation in MGC-803 cells and NRK cells[16]. It has been known that TSPAN4 remains stable on the migrasome membrane[17]. However, it remains to be explored whether there is a mechanism targeted TSPAN4 for degradation in the cytoplasm, which could negatively regulate migrasome formation. Members of the tetraspanin family are known to play important roles in viral entry, as TSPAN9 has been implicated in alphavirus entry, TSPAN8 is essential for coronavirus entry, TSPAN27 is involved in HTLV-1 entry, and CD81 serves as the receptor for HCV[18–25]. However, the role of TSPAN4 in viral release has not been explored.

O-linked *N*-acetylglucosamine (*O*-GlcNAc) glycosylation, also known as *O*-GlcNAcylation, is a dynamic post-translational modification that involves the attachment of single *O*-GlcNAc moieties to serine (Ser) and threonine (Thr) residues of various proteins to respond promptly to internal and external cues through direct and dynamic regulation of protein functions[26]. *O*-GlcNAc transferase (OGT) and *O*-GlcNAcase (OGA) function together and control the dynamic cycling of this modification in a nutrient or stress-responsive manner[27]. A previous study indicated that TSPAN4-GFP appears as a smeared double band on Western blots (WB), which was suggested to be a result of glycosylation, although this claim was not supported by further experimental investigation [16].

In this study, we report that *O*-GlcNAcylation of AMFR-mediated by OGT serves as a regulatory mechanism for AMFR-mediated TSPAN4 degradation and migrasome formation. Additionally, migrasomes can facilitate viral release and spread among neighboring cells. By leveraging the AMFR-TSPAN4 axis, Vesicular stomatitis virus (VSV) or HSV-1 infection initially promotes migrasome formation to facilitate viral release during the early stage of infection, when only a limited number of progeny viruses are produced, and subsequently suppresses migrasome formation during the late stage of infection, when a substantial quantity of viral particles is generated.

Results

Viruses use migrasomes for release and spread

Given that the primary function of migrasomes is their ability to serve as packets of delivery, we proposed that viruses may utilize migrasomes for their release and spread. We first overexpressed the mammalian tetraspanins TSPAN1, TSPAN2, or TSPAN4, which have been identified for their ability to induce migrasome formation[16]. Overexpression of TSPAN1, TSPAN2, or TSPAN4 enhanced the replication of RNA virus VSV, while the expression of TSPAN8 or TSPAN19 neither promoted migrasome formation nor regulated virus replication (Supplementary Fig. 1a) [16].

Since TSPAN4 is one of the most effective tetraspanins for both migrasome induction and virus replication, we chose it for in-depth study. To study the role of TSPAN4 in viral release, we first confirmed that overexpression or knockdown of TSPAN4 had minor effect on IFNβ production (Supplementary Fig. 1b). When infected with the RNA virus VSV or the DNA virus Herpes simplex virus 1 (HSV-1) at a low multiplicity of infection (MOI) of 0.01, extracellular viral production (virions released into the supernatant) was significantly enhanced in TSPAN4-overexpressing cells, whereas it was reduced in *Tspan4* knockout cells (Fig. 1a, b). Through attachment and internalization assays, we further demonstrated that neither TSPAN4 overexpression nor *Tspan4* knockout affected the entry of VSV or HSV-1 (Supplementary Fig. 1c, d). Additionally, we disrupted migrasome formation using previously reported strategies, such as the knockdown of Cert, Ceramide synthases 5 (CerS5), Sgms2, PIP5K1A, or Rab35[17,28], and the data showed that the impairment of migrasome formation led to decreased viral release (Fig. 1c, d). Thus, these data support the conclusion that migrasomes facilitate viral release.

Next, we aim to investigate how migrasomes function in viral release. We first purified migrasomes from VSV-infected cells and found that the viral protein M was detectable in the migrasome fraction (Fig. 1e). We further used these purified migrasomes to infect mock cells, and found that these migrasomes were infectious (Fig. 1f). Notably, the VSV-GFP signal was observed inside the migrasomes in VSV-infected cells (Fig. 1f). Similar results were obtained by detecting the HSV-1 virion signal using a viral N antibody (Supplementary Fig. 1e). Furthermore, using transmission electron microscopy (TEM), we directly visualized hexagonal virus particles within the migrasomes from VSV-infected cells (Fig. 1g). These results indicate that viral particles were enriched in migrasomes.

Interestingly, using live imaging, we observed that when a non-infected cell migrated, it can uptake the virions contained-migrasomes left by neighboring VSV-infected cell, subsequently leading to infection (Fig. 1h and Supplementary Movie 1). VSV-G protein is known to mediate membrane fusion during the infection process[29]. We subsequently investigated whether the VSV-G protein could translocate to the migrasome membrane to facilitate the membrane fusion between virus-containing migrasomes and cellular membrane, thereby enabling viral transmission. Using proteinase K protection assay and confocal microscopy, we confirmed that VSV-G protein was partly enriched on the out membrane of migrasomes (Supplementary Fig. 1f, g). We subsequently treated the purified migrasomes isolated from VSV-infected cells with proteinase K to degrade the migrasome outer membrane-localized VSV-G. These treated migrasomes were then incubated with control cells. Compared to the PBS-treated control, migrasomes treated with proteinase K alone exhibited a slightly reduction in infectivity, whereas co-treatment with proteinase K and Triton ×-100 abolished migrasome-mediated infectivity (Fig. 1i), indicating that the primary mechanism of migrasome-mediated viral transmission is mediated by VSV virions contained inside the migrasomes, whereas the VSV-G protein localized on the outer membrane of migrasomes contributes only minimally to this process. Collectively, these data indicate an interesting way for viral spread mediated by migrasomes.

TSPAN4 is degraded via ubiquitin-proteasome pathway

Strikingly, we observed a cumulative decrease in migrasome formation as the infection progressed (Fig. 1j, k). TSPAN4 is known to be critical for migrasome formation, as its gain and loss lead to a corresponding increase and decrease in migrasome formation[16]. We then carefully examined the protein levels of TSPAN4 in virus-infected cells. The amount of TSPAN4 initially increased and then dramatically decreased at increasing intervals of time following VSV or HSV-1 infection (Fig. 1l, m). Hence, virus infection dynamically regulates the protein levels of TSPAN4.

To investigate how viruses regulate TSPAN4 expression, we first treated TSPAN4-Flag stably expressing cells with Cycloheximide (CHX) to inhibit protein synthesis, and found that TSPAN4-Flag was remarkably degraded following CHX treatment, even after just 30 min (Fig. 2a). To better understand the mechanism underlying TSPAN4 degradation, we inhibited the ubiquitin-proteasome pathway using MG132 and the autophagosome-lysosome pathway using Chloroquine (CQ). MG132 treatment significantly while CQ treatment only slightly blocked TSPAN4-Flag degradation (Fig. 2b), indicating that TSPAN4 can be degraded via the ubiquitin-proteasome pathway. Additionally, virus infection-induced TSPAN4 degradation was also blocked by MG132 treatment (Fig. 2c, d). We further found that TSPAN4 undergoes K48-linked polyubiquitination, and the mutant, which lacks amino acids 106–238, completely lost its ubiquitination capability (Fig. 2e, f). Six lysine residues are located within the 106–238 region of TSPAN4 (Fig. 2g). Our observations indicated that all six lysine residues are essential for TSPAN4 ubiquitination, as the point mutant 6 K/R (abbreviated as TSPAN4^{6KR}) completely abolished ubiquitin modification (Fig. 2g, h). TSPAN4^{6KR} exhibited greater stability than the

https://doi.org/10.1038/s41467-025-68220-3

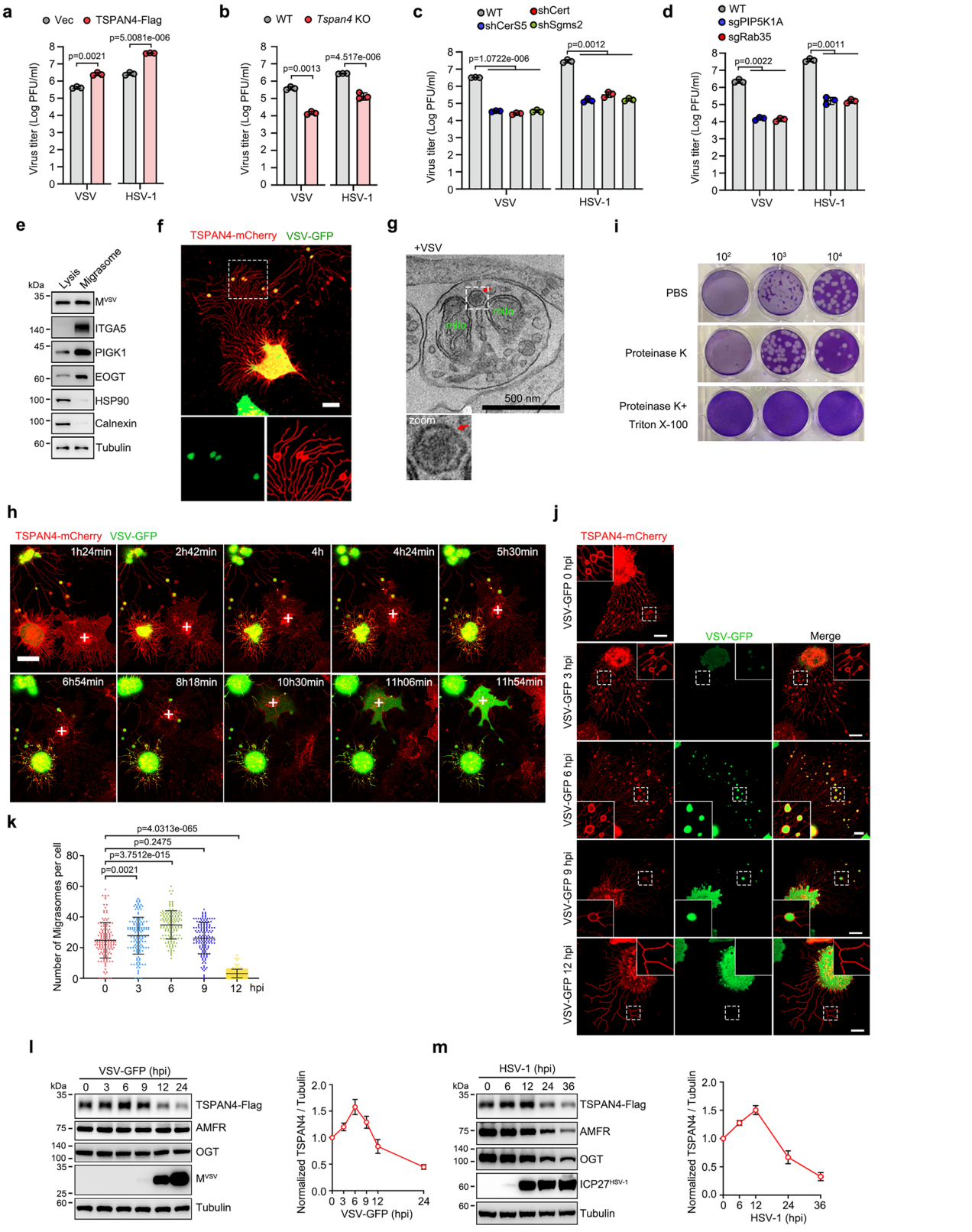

wild-type in the CHX assay (Fig. 2i). Together, these data indicate that TSPAN4 is subject to ubiquitination and subsequent degradable.

TSPAN4 is degraded on ER by AMFR-catalyzed K48-linked polyubiquitination

To identify the E3 ligase responsible for the ubiquitination of TSPAN4, we conducted immunoprecipitation-mass spectrometry (IP/MS) using TSPAN4-Flag as the bait (Supplementary Fig. 2a and Supplementary Data 1). Several candidates related to ubiquitin were identified (Supplementary Fig. 2b). We then performed a small-scale RNA interference (RNAi) screening targeting these candidates, and found that knockdown of autocrine motility factor receptor (AMFR, also known as GP78 or RNF45) significantly inhibited the degradation of TSPAN4-Flag in the CHX assay (Supplementary Fig. 2c). AMFR is an ER transmembrane

Fig. 1 | Migrasomes facilitate viral release. a NRK cells stably expressing Vector or TSPAN4-Flag were infected with VSV-GFP (Multiplicity of infection (MOI) = 0.01) or HSV-1 (MOI = 0.01) and incubated for an additional 12 or 36 h. Culture supernatants were collected, and viral titers were quantified using plaque assays. Data represent the mean ± SD from three biological replicates. Statistical significance was determined using a two-tailed Student's *t*-test. Source data are provided as a Source Data file. **b** Wild-type (WT) or *Tspan4* Knockout (KO) NRK cells were infected with VSV-GFP (MOI = 0.01) or HSV-1 (MOI = 0.01) and incubated for an additional 12 or 36 h. Culture supernatants were collected, and viral titers were quantified using plaque assays. Data represent the mean ± SD from three biological replicates. Statistical significance was determined using a two-tailed Student's *t*-test. Source data are provided as a Source Data file. **c** L929 cells stably expressing TSPAN4-Flag were infected with lentivirus carrying constructs with non-specific shRNA or shRNA targeting Cert, Cers5, or Sgsm2, cells were infected with VSV-GFP (MOI = 0.01) or HSV-1 (MOI = 0.01) and incubated for an additional 12 or 36 h. Culture supernatants were collected, and viral titers were quantified using plaque assays. Data represent the mean ± SD from three biological replicates. Statistical significance was determined using a two-tailed Student's *t*-test. Source data are provided as a Source Data file. **d** WT, *PIP5K1A* or *Rab35* KO NRK-TSPAN4-Flag cells were infected with VSV-GFP (MOI = 0.01) or HSV-1 (MOI = 0.01) and incubated for an additional 12 or 36 h. Culture supernatants were collected, and viral titers were quantified using plaque assays. Data represent the mean ± SD from three biological replicates. Statistical significance was determined using a two-tailed Student's *t*-test. Source data are provided as a Source Data file. **e** L929 cells stably expressing TSPAN4-mCherry were infected with VSV-GFP at an MOI of 0.2. Samples from cell bodies and purified migrasomes were analyzed via WB using antibodies against VSV-M, HSP90, Calnexin, Tubulin, and identified migrasome-specific marker ITGA5, PIGK, and EOGT ($n = 3$ independent experiments). Source data are provided as a Source Data file. **f** NRK cells stably expressing TSPAN4-mCherry were incubated with purified migrasomes from. **e** ($n = 3$ independent experiments). Cells were imaged by confocal microscopy. Green, VSV-GFP; red, TSPAN4-mCherry. Scale bar represents 10 μm. **g** Representative transmission electron micrograph (TEM) images of VSV-GFP (at an MOI of 0.2) infected NRK cells ($n = 3$ independent experiments). Red arrows indicated virions in migrasomes. Mito, mitochondria. Scar bar represents 500 nm. **h** Time-lapse imaging of VSV-GFP (at an MOI of 0.2) infected NRK cells stably expressing TSPAN4-mCherry. Images were captured every 6 min by confocal microscopy. Green, VSV-GFP; red, TSPAN4-mCherry. Scale bar, 10 μm. **i** Representative images from plaque assay of three biological replicates from purified migrasomes (from VSV-GFP infected TSPAN4-mCherry stably expressing L929 cells) treated with either Proteinase K, Proteinase K and Triton ×-100, or PBS. Source data are provided as a Source Data file. **j**, **k** NRK cells stably expressing TSPAN4-mCherry were infected with VSV-GFP at an MOI of 0.2 for the indicated time. Cells were imaged by confocal microscopy. Green, VSV-GFP; red, TSPAN4-mCherry. Scar bar represents 10 μm. Number of migrasomes from the cells in (**i**); $n = 150$ cells for 0 h, $n = 150$ cells for 3 h, $n = 149$ cells for 6 h, $n = 150$ cells for 9 h, and $n = 150$ cells for 12 h per group from three independent experiments. Error bars, mean ± SD. Source data are provided as a Source Data file. **l**, **m** HeLa cells stably expressing TSPAN4-Flag were infected with VSV-GFP or HSV-1 at an MOI of 1 for indicated time. Lysates were analyzed via WB. Relative intensity of TSPAN4 normalized to Tubulin of three independent experiments was quantified. Error bars, mean ± SD. Source data are provided as a Source Data file.

protein that functions as a ubiquitin E3 ligase in ER-associated protein degradation[30]. Using a co-immunoprecipitation (co-IP) assay, we confirmed that TSPAN4 interacts with AMFR (Fig. 3a). The direct interaction between TSPAN4 and AMFR was further validated through an in vitro GST pull-down assay (Fig. 3b). Colocalization of TSPAN4 and AMFR was observed in cells treated with or without fibronectin (Supplementary Fig. 2d). Overexpression of wild-type AMFR, but not the catalytically inactive mutant AMFR C341/356/378S (abbreviated as $AMFR^{3CS}$), increased the ubiquitination level of TSPAN4 (Fig. 3c and Supplementary Fig. 2e). The kinetics of AMFR expression correlated with the increase in wild-type TSPAN4 degradation, but not with $TSPAN4^{6KR}$ (Fig. 3d). Overexpression of $AMFR^{3CS}$ failed to induce TSPAN4 degradation (Fig. 3e and Supplementary Fig. 2f). Next, we generated *Amfr* knockout (KO) cells and found that, compared to wild-type cells, TSPAN4 was more stable in *Amfr* KO cells in the CHX assay (Fig. 3f). Furthermore, we conducted the rescue experiments and found that wild-type AMFR, but not $AMFR^{3CS}$, restored the degradation of TSPAN4 in *Amfr* KO cells (Fig. 3g). Thus, AMFR is the E3 ligase responsible for TSPAN4 degradation.

Given that AMFR is an ER-resident E3 ligase, and TSPAN4 was partially localized on the ER (Supplementary Fig. 2g). We first quantified the proportion of TSPAN4 localized in the ER relative to its total cellular pool, and found that 32.12 ± 2.31% of total TSPAN4 was enrich in the ER (Supplementary Fig. 2g, h). To further explore the mechanism by which AMFR degrades TSPAN4, we analyzed the TSPAN4 stability in the ER fraction and non-ER fraction from cells overexpressing either AMFR or $AMFR^{3CS}$. Only the ER-localized TSPAN4 was degraded upon AMFR overexpression, while the non-ER TSPAN4 remained stable (Fig. 3h). Furthermore, AMFR exhibited no co-localization with cell membrane-localized TSPAN4 (Supplementary Fig. 2i). Thus, these findings suggest that TSPAN4 can be degraded in the ER through AMFR-mediated ubiquitin-proteasome pathways.

Interestingly, we noticed that TSPAN4 degradation induced by AMFR can be significantly blocked by MG132 treatment, and also partly blocked by CQ treatment (Supplementary Fig. 2j), indicating that beside ubiquitin-proteasome, autophagosome-lysosome may function as alternative pathways to AMFR-mediated degradation contribute to TSPAN4 turnover.

AMFR regulates migrasome formation by modulating TSPAN4 stability

Next, we investigated whether AMFR can modulate migrasome formation by inducing the degradation of ER-localized TSPAN4. We first confirmed that AMFR expression does not affect the speed of cell migration (Fig. 3i). ITGA5-mCherry was used as the migrasome marker, and confocal microscopy data revealed that overexpression of AMFR-GFP, but not $AMFR^{3CS}$-GFP or GFP, resulted in a decreased number of migrasomes (Fig. 3j, k). We observed that AMFR was not localized on migrasomes, further confirming that AMFR does not mediate the degradation of migrasome-localized TSPAN4 (Fig. 3j). Additionally, we conducted the rescue experiments in *Tspan4* KO cells, and found that overexpression of AMFR, but not $AMFR^{3CS}$-GFP, induced TSPAN4 degradation and abolished the migrasome formation that was rescued by wild-type TSPAN4 overexpression. In contrast, overexpression of either AMFR or $AMFR^{3CS}$ had a minor effect on the TSPAN4 stability and migrasome formation rescued by $TSPAN4^{6KR}$ expression (Fig. 3l–n). Together, these results suggest that AMFR functions as the E3 ligase that mediates the degradation of ER-localized TSPAN4, thereby preventing the formation of migrasomes.

O-GlcNAcylation regulates TSPAN4 stability and migrasome formation

Next, we investigated the regulatory mechanism by which TSPAN4 is degraded by AMFR. A previous study indicated that TSPAN4 may undergo *O*-GlcNAcylation[16]. We then aimed to determine whether *O*-GlcNAcylation regulate migrasome formation. Treatment with the OGA inhibitor Thiamet G (TMG) slightly increased the number of migrasomes, while treatment with the OGT inhibitor OSMI-1 obviously impaired migrasome formation (Fig. 4a, b). Consistently, knockdown of *O*-GlcNAc transferase OGT obviously inhibited migrasome formation (Fig. 4c, d). We further conducted rescue experiments in OGT KD cells and found that wild-type OGT, but not the catalytic dead mutant OGT^{K852M}, restored the formation of migrasomes (Fig. 4c, d)[31]. Thus, *O*-GlcNAcylation facilitates migrasome formation.

We then investigated whether *O*-GlcNAcylation regulate the stability of TSPAN4. TMG slightly enhanced, while OSMI-1 treatment decreased the protein level of TSPAN4, suggesting that *O*-

https://doi.org/10.1038/s41467-025-68220-3

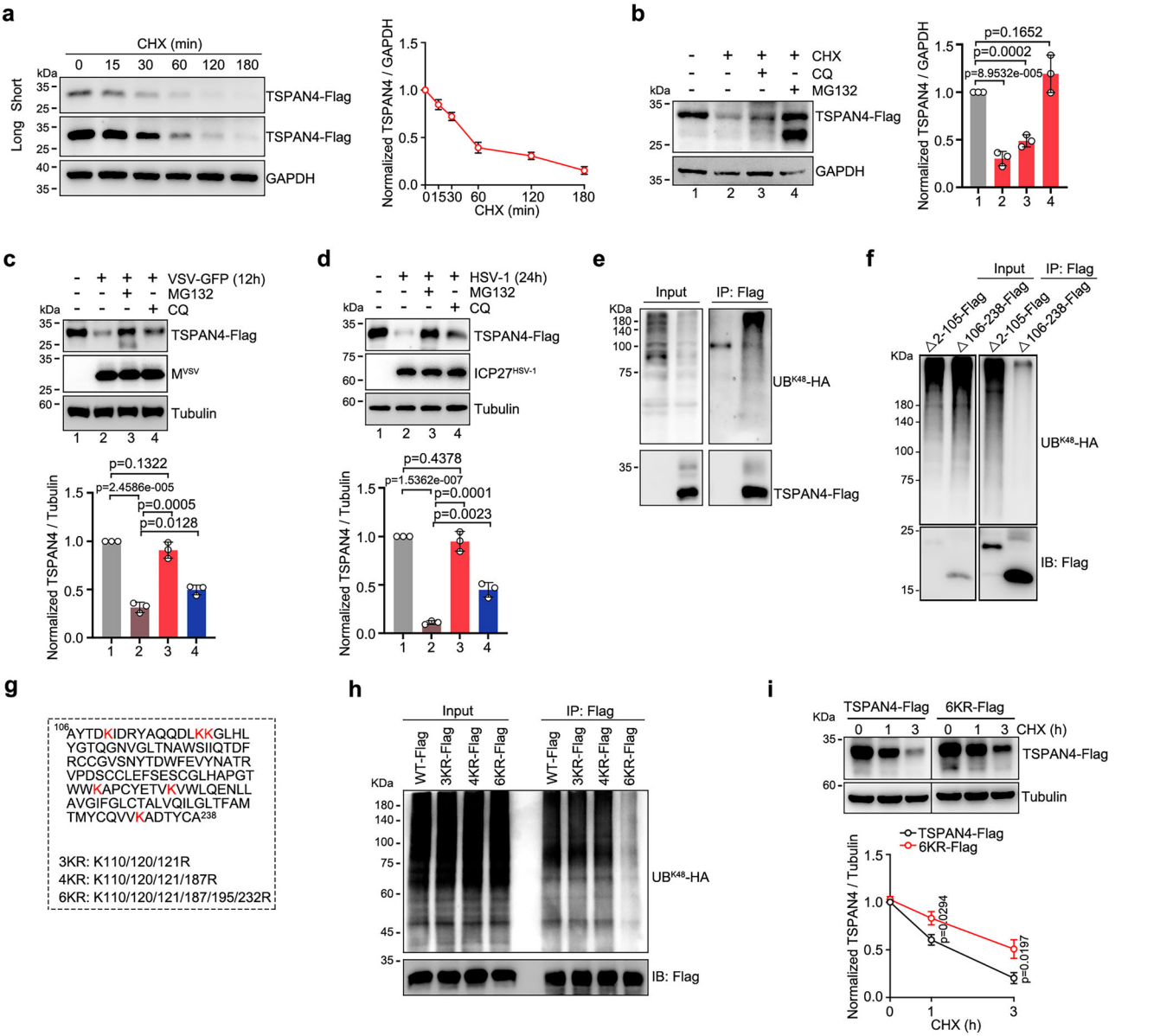

Fig. 2 | TSPAN4 is ubiquitinated for degradation. a HeLa cells stably expressing TSPAN4-Flag were treated with 100 μM CHX for indicated time. Lysates were analyzed via WB. Relative intensity of TSPAN4 normalized to GAPDH of three independent experiments was quantified. Error bars, mean ± SD. Source data are provided as a Source Data file. **b** HeLa cells stably expressing TSPAN4-Flag were treated with 100 μM CHX for 1 h, and further treated with 100 μM CQ or 10 μM MG132 for 6 h. Lysates were analyzed via WB. Relative intensity of TSPAN4 normalized to GAPDH of three independent experiments was quantified. Error bars, mean ± SD. Two-tailed Unpaired Student's *t*-test. Source data are provided as a Source Data file. **c**, **d** HeLa cells stably expressing TSPAN4-Flag were infected with or without VSV-GFP or HSV-1 at an MOI of 1 for indicated time, and were further treated with or without 10 μM MG132 or 100 μM CQ for 6 h. Lysates were analyzed via WB. Relative intensity of TSPAN4 normalized to Tubulin of three independent experiments was quantified. Error bars, mean ± SD. Two-tailed Unpaired Student's *t*-test. Source data are provided as a Source Data file. **e** HEK293T cells were transfected with HA-Ub^{K48} with or without TSPAN4-Flag for 36 h. Interactions were analyzed by co-immunoprecipitation ($n = 3$ independent experiments). Source data are provided as a Source Data file. **f** HEK293T cells were transfected with HA-Ub^{K48} and TSPAN4-Flag mutants for 36 h. Interactions were analyzed by co-immunoprecipitation ($n = 3$ independent experiments). Source data are provided as a Source Data file. **g** Amino acid sequence from 106 to 238 of TSPAN4 and point mutations used in this study. **h** 6 K (K110, K120, K121, K187, K195, K232) are the main ubiquitin site of TSPAN4. HEK293T cells were transfected with HA-Ub^{K48} and TSPAN4-Flag or its mutants for 36 h. Interactions were analyzed by co-immunoprecipitation ($n = 3$ independent experiments). Source data are provided as a Source Data file. **i** HeLa cells were transfected with TSPAN4-Flag or TSPAN4^{6KR}-Flag for 24 h, and cells were further treated with 100 μM CHX for indicated time. Lysates were analyzed via WB. Relative intensity of TSPAN4 normalized to Tubulin of three independent experiments was quantified. Error bars, mean ± SD. Two-tailed Unpaired Student's *t*-test. Source data are provided as a Source Data file.

GlcNAcylation may inhibit the degradation of TSPAN4 (Supplementary Fig. 3a). Overexpression of wild-type OGT, but not the OGT^{K852M} mutant, attenuated TSPAN4 degradation in the CHX assay (Fig. 4e). Additionally, knockdown of OGT promoted TSPAN4 degradation, which could be blocked by treatment with MG132 (Fig. 4f). Rescue experiments in OGT KD cells demonstrated that expression of wild-type OGT, but not OGT^{K852M} mutant, reversed the degradation of TSPAN4 (Fig. 4g). Thus, OGT stabilizes TSPAN4 dependent on its transferase activity.

We then tested whether *O*-GlcNAcylation regulate the stability of TSPAN4 through its ubiquitination. Treatment with TMG significantly reduced TSPAN4 ubiquitination, while treatment with OSMI-1 enhanced it (Fig. 4h, i). Consistently, we observed that the ubiquitination of TSPAN4 increased upon OTG knockdown, whereas it

https://doi.org/10.1038/s41467-025-68220-3

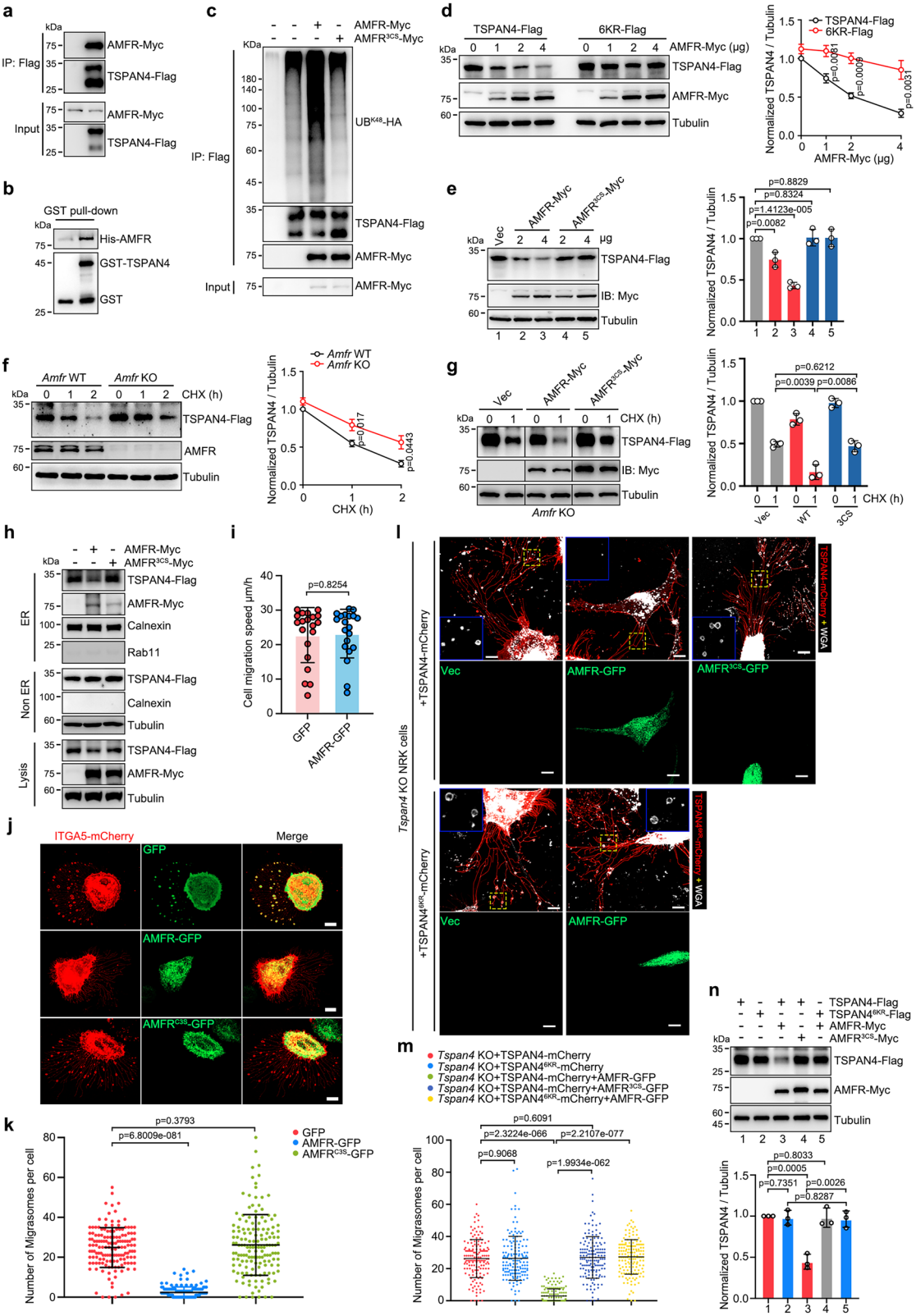

decreased under OGT overexpression conditions, but not with OGT^{K852M} overexpression (Fig. 4j, k). Together, these data indicate that *O*-GlcNAcylation inhibits the ubiquitination of TSPAN4, thereby enhancing its stability to facilitate migrasome formation.

O-GlcNAcylation of AMFR at T643

Next, we sought to determine the mechanism(s) by which *O*-GlcNAcylation regulate migrasome formation. Using an anti-*O*-GlcNAc antibody, we unexpectedly found that AMFR, but not TSPAN4, was *O*-GlcNAcylated (Fig. 5a). The level of AMFR *O*-GlcNAcylation was increased following TMG treatment, while it decreased under OSMI-1 treatment (Supplementary Fig. 3b, c). Through in vivo co-IP and in vitro GST pull-down assays, we confirmed that AMFR directly interacts with the *O*-GlcNAcylation enzyme OGT (Fig. 5b, c). In vitro, *Escherichia coli* expressed His-tagged AMFR was incubated with recombinant wild-type glutathione S-transferase (GST)-tagged OGT or the catalytic dead

Fig. 3 | AMFR mediates the K48-linked TSPAN4 ubiquitination to regulate migrasome formation. a Co-immunoprecipitation analysis of TSPAN4-Flag with AMFR-Myc in HEK293T cells ($n = 3$ independent experiments). Source data are provided as a Source Data file. **b** Purified His-AMFR was incubated with purified GST or GST-TSPAN4, and analysis of the interactions between AMFR and TSPAN4 by in vitro GST pull-down was performed ($n = 3$ independent experiments). Source data are provided as a Source Data file. **c** AMFR overexpression enhances the ubiquitin level of TSPAN4. HEK293T cells were transfected with TSPAN4-Flag, HA-Ub^{K48}, and AMFR-Myc or mutant $AMFR^{3CS}$-Myc for 36 h. Lysates were subjected to Flag immunoprecipitation and analyzed via WB ($n = 3$ independent experiments). Source data are provided as a Source Data file. **d** HeLa cells were transfected with indicated plasmids for 24 h, and lysates were analyzed via WB. Relative intensity of TSPAN4 and $TSPAN4^{6KR}$ of three independent experiments normalized to Tubulin, was quantified. Error bars, mean ± SD. Two-tailed Unpaired Student's *t*-test. Source data are provided as a Source Data file. **e** HeLa cells stably expressing TSPAN4-Flag were transfected with gradient AMFR-Myc or point mutant $AMFR^{3CS}$-Myc for 24 h. Lysates were analyzed via WB. Relative intensity of TSPAN4 of three independent experiments normalized to Tubulin, was quantified. Error bars, mean ± SD. Two-tailed Unpaired Student's *t*-test. Source data are provided as a Source Data file. **f** WT or *Amfr* KO HeLa cells stably expressing TSPAN4-Flag were treated with 100 μM CHX for indicated time. Lysates were analyzed via WB. Relative intensity of TSPAN4 of three independent experiments normalized to Tubulin, was quantified. Error bars, mean ± SD. Two-tailed Unpaired Student's *t*-test. Source data are provided as a Source Data file. **g** *Amfr* KO HeLa cells stably expressing TSPAN4-Flag were transfected with AMFR-Myc or $AMFR^{3CS}$-Myc for 24 h, and harvested before 1 h with or without 100 μM CHX treatment. Lysates were analyzed via WB. Relative intensity of TSPAN4 of three independent experiments normalized to Tubulin, was quantified. Error bars, mean ± SD. Two-tailed Unpaired Student's *t*-test. Source data are provided as a Source Data file. **h** Subcellular fractions were isolated from HeLa cells stably expressing TSPAN4-Flag transfected with AMFR-Myc or $AMFR^{3CS}$-Myc. Calnexin represent the ER, Rab11 represent endosomes, and Tubulin represents cytoplasm, respectively. Source data are provided as a Source Data file. **i** Quantification of the migration speed of GFP or AMFR-GFP expressing NRK cells. 20 cells of two independent experiments were counted. Error bars, mean ± SD. Two-tailed Unpaired Student's *t*-test. Source data are provided as a Source Data file. **j**, **k** NRK-ITGA5-mCherry cells were transfected with GFP, AMFR-GFP, or $AMFR^{3CS}$-GFP. Cells were imaged by confocal microscopy. Green, GFP, AMFR-GFP, and $AMFR^{3CS}$-GFP; red, ITGA5-mCherry; yellow, Merge. Number of migrasomes from the cells in (**j**); $n = 150$ cells per group from three independent experiments. Scar bar represents 10 μm. Error bars, mean ± SD. Two-tailed Unpaired Student's *t*-test. Source data are provided as a Source Data file. **l**, **m** *Tspan4* KO NRK cells were transfected with TSPAN4-mCherry or $TSPAN4^{6KR}$-mCherry, with or without GFP, AMFR-GFP, or $AMFR^{3CS}$-GFP. Wheat germ agglutinin (WGA) was used to stain migrasomes. Green, Vec, AMFR-GFP and $AMFR^{3CS}$-GFP; red, TSPAN4-mCherry and $TSPAN46^{KR}$-mCherry; white, Migrasomes. Scar bar represents 10 μm. Cells were imaged by confocal microscopy. Number of migrasomes from the cells in (**l**); $n = 150$ cells per group from three independent experiments. Error bars, mean ± SD. Two-tailed Unpaired Student's *t*-test. Source data are provided as a Source Data file. **n** *Tspan4* KO Hela cells were transfected with the indicated plasmids for 24 h. Lysates were analyzed via WB. Relative intensity of TSPAN4 and $TSPAN4^{6KR}$ of three independent experiments normalized to Tubulin, was quantified. Error bars, mean ± SD. Two-tailed Unpaired Student's *t*-test. Source data are provided as a Source Data file.

mutant GST-OGT^{K852M}, along with UDP-GlcNAc, and subjected to an *O*-GlcNAcylation assay. We found that wild-type OGT, but not the OGT^{K852M} mutant, catalyzed the *O*-GlcNAcylation of AMFR (Fig. 5d). Noticeably, AMFR *O*-GlcNAcylation was abolished by co-incubation with OGA (Fig. 5e). In cellular experiments, the amount of *O*-GlcNAc-modified AMFR was lower in OGT KD cells compared to controls (Fig. 5f), whereas overexpression of wild-type OGT, but not OGT^{K852M}, promoted AMFR *O*-GlcNAcylation (Fig. 5g). Consistently, co-expression of OGA impaired OGT-mediated AMFR *O*-GlcNAcylation in cells (Fig. 5g).

We then sought to unambiguously identify the *O*-GlcNAcylation site(s) on AMFR. Based on predictions for *O*-GlcNAcylation attachment sites in YinOYang[32], six potential *O*-GlcNAcylation sites were identified (Fig. 5h). To comprehensively map these possible sites, we generated point mutations at the indicated residues. Notably, T643A mutation significantly reduced AMFR *O*-GlcNAcylation, while other mutations had minimal impact (Fig. 5i, j). Through mass spectrometry analysis of the synthesized AMFR peptide, we further confirmed that AMFR T643 can be *O*-GlcNAcylated (Fig. 5k). Therefore, both mass spectrometry and extensive mutation studies suggested that T643 is the primary *O*-GlcNAcylation site on AMFR.

We were surprised found that T643 is not evolutionarily conserved (Supplementary Fig. 3d). Except mouse and rat, in other species, such as *Homo sapiens* the last amino acid is Ser. We then verified whether the last amino acid Ser of human AMFR (abbreviated as hAMFR) can also be *O*-GlcNAcylated. In vivo and in vitro assays suggested that $hAMFR^{S643A}$ showed reduced *O*-GlcNAcylation, suggesting that S643 of human AMFR is the primary site for *O*-GlcNAcylation (Supplementary Fig. 3e, f).

O-GlcNAcylation of AMFR at T643 stabilizes TSPAN4 for migrasome formation

Next, we sought to determine whether *O*-GlcNAcylation of AMFR regulate TSPAN4 degradation and migrasome formation. We first treated cells with the OGT inhibitor OSMI-1 or the OGA inhibitor TMG and examined TSPAN4 degradation and migrasome formation. OSMI-1 treatment resulted in increased AMFR-mediated TSPAN4 degradation and reduced migrasome formation, whereas TMG treatment partially impaired AMFR-mediated TSPAN4 degradation and the defect of migrasome formation (Supplementary Fig. 3g–j). Neither OSMI-1 nor TMG treatment had any effect on $AMFR^{T643A}$-induced TSPAN4 degradation or on $AMFR^{T643A}$-inhibited migrasome formation (Supplementary Fig. 3g–j).

Furthermore, we noticed that co-expression of OGT reversed AMFR (but not $AMFR^{T643A}$)-abolished migrasome formation (Fig. 5l, m). Consistently, co-expression of OGT restored TSPAN4 degradation induced by AMFR, but did not affect TSPAN4 degradation induced by $AMFR^{T643A}$ (Fig. 5n).

Together, these observations demonstrate that *O*-GlcNAcylation of AMFR at T643 suppresses the degradation of TSPAN4 and facilitates migrasome formation.

O-GlcNAcylation of AMFR disrupts AMFR-TSPAN4 interactions

Next, we sought to determine the mechanism(s) by which *O*-GlcNAcylation of AMFR inhibit TSPAN4 degradation. We first assayed whether the TSPAN4-AMFR interactions were affected by *O*-GlcNAcylation. Indeed, TSPAN4-AMFR interactions were suppressed upon TMG treatment (Supplementary Fig. 3k). Conversely, OSMI-1 treatment enhanced TSPAN4-AMFR interactions (Supplementary Fig. 3l). We further found that knockdown of OGT enhanced AMFR-TSPAN4 interactions (Fig. 5o), whereas overexpression of wild-type OGT, but not OGT^{K852M} mutant, disrupted AMFR-TSPAN4 interactions (Fig. 5p). OGT overexpression failed to affect the interactions between $AMFR^{T643A}$ and TSPAN4 (Fig. 5Q). Consistently, human TSPAN4-AMFR interactions were also affected by *O*-GlcNAcylation in cells (Supplementary Fig. 3m, n). Furthermore, His-AMFR recombinantly expressed and purified from *Escherichia coli* was incubated with OGT and UDP-GlcNAc to elevate the level of *O*-GlcNAcylation. In vitro pull-down of the differentially *O*-GlcNAcylated AMFR proteins with recombinant TSPAN4 showed that upregulated *O*-GlcNAcylation blocked AMFR-TSPAN4 interactions (Fig. 5r). To further investigate the molecular mechanism by which *O*-GlcNAcylation disrupts the AMFR-TSPAN4 interaction, we employed AlphaFold to predict the structure of the AMFR-TSPAN4 complex and generated an AMFR mutant (W345A/E634A/H420A/R484A/R428A/F424A/F436A) lacking the putative TSPAN4-binding domain (Supplementary Fig. 3o). This AMFR mutant

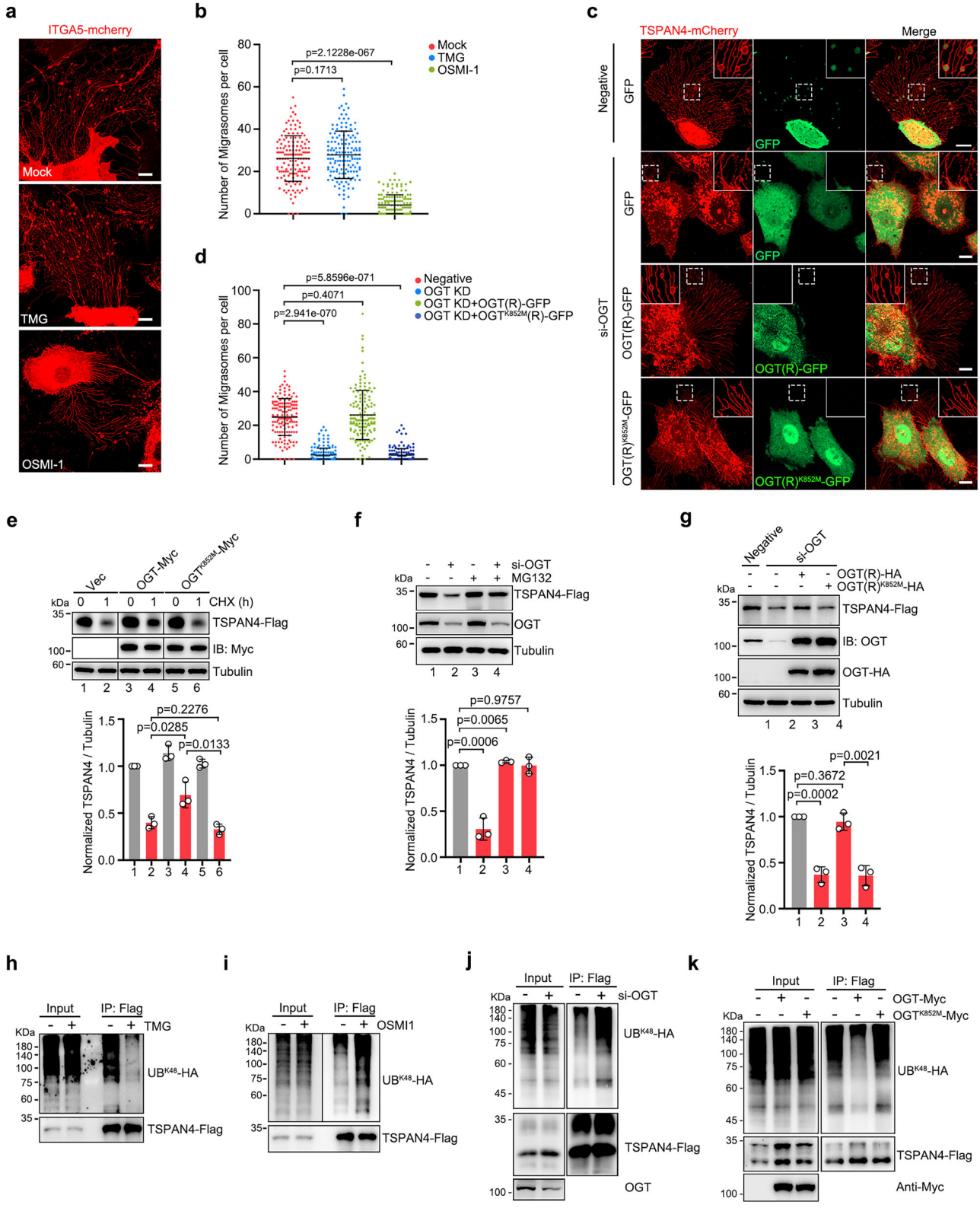

exhibited significantly reduced binding affinity toward TSPAN4 (Supplementary Fig. 3p), supporting the reliability of the structural prediction. Given that the potential *O*-GlcNAcylation site is located in proximity to the AMFR-TSPAN4 interaction interface, we hypothesize that *O*-GlcNAcylation at residue T643 may induce steric hindrance, thereby disrupting the AMFR-TSPAN4 association.

Put together, these results support a mechanism in which OGT-mediated *O*-GlcNAcylation of AMFR attenuates AMFR-TSPAN4 interactions, and this inhibition subsequently prevents AMFR-mediated ubiquitination and degradation of TSPAN4, thereby facilitating migrasome formation.

AMFR-TSPAN4 axis regulates viral release

Given that AMFR *O*-GlcNAcylation and TSPAN4 ubiquitination regulate migrasome formation and migrasomes facilitate viral release and spread, we aimed to determine whether the AMFR-TSPAN4 axis

Fig. 4 | *O*-GlcNAcylation regulates TSPAN4 degradation and migrasome formation. a, **b** NRK cells expressing ITGA5-mCherry were treated with 10 μM TMG or 50 μM OSMI-1 for 6 h. Cells were imaged by confocal microscopy. Red, ITGA5-mCherry. Number of migrasomes from the cells in (**a**); $n = 150$ cells per group from three independent experiments. Scar bar represents 10 μm. Error bars, mean ± SD. Two-tailed Unpaired Student's *t*-test. Source data are provided as a Source Data file. **c**, **d** NRK-TSPAN4-mCherry cells were transfected with negative siRNA or OGT siRNA for 24 h, and cells were further transfected with GFP, RNAi-resistant OGT(R)-GFP or OGT(R)^{K852M}-GFP for another 24 h. Cells were imaged by confocal microscopy. Green, GFP, OGT(R)-GFP and OGT(R)^{K852M}-GFP; red, TSPAN4-mCherry; yellow, Merge. Number of migrasomes from the cells in (**c**); $n = 150$ cells per group from three independent experiments. Scar bar represents 10 μm. Error bars, mean ± SD. Two-tailed Unpaired Student's *t*-test. Source data are provided as a Source Data file. **e** HeLa cells stably expressing TSPAN4-Flag were transfected with indicated plasmids for 24 h, and cells were treated with or without 100 μM CHX for 1 h. Lysates were analyzed via WB. Relative intensity of TSPAN4 of three independent experiments normalized to Tubulin, was quantified. Error bars, mean ± SD. Two-tailed Unpaired Student's *t*-test. Source data are provided as a Source Data file. **f** HeLa cells stably expressing TSPAN4-Flag were transfected with or without OGT siRNA for 48 h, and before harvested, cells were supplemented with or without 10 μM MG132 for 6 h. Lysates were analyzed via WB. Relative intensity of TSPAN4 of three independent experiments normalized to Tubulin, was quantified. Error bars, mean ± SD. Two-tailed Unpaired Student's *t*-test. Source data are provided as a Source Data file. **g** HeLa cells stably expressing TSPAN4-Flag were transfected with or without OGT siRNA for 24 h, and cells were further transfected with OGT(R)-HA or OGT(R)^{K852M}-HA for 24 h. Lysates were analyzed via WB. Relative intensity of TSPAN4 of three independent experiments normalized to Tubulin, was quantified. Error bars, mean ± SD. Two-tailed Unpaired Student's *t*-test. Source data are provided as a Source Data file. **h**, **i** Analysis of the interactions between TSPAN4-Flag and Ub^{K48}-HA treated with 10 μM TMG or 50 μM OSMI-1 for 6 h via co-immunoprecipitation assay ($n = 3$ independent experiments). Source data are provided as a Source Data file. **j** HEK293T cells were transfected with or without OGT siRNA for 12 h, and cells were further transfected with Ub^{K48}-HA and TSPAN4-Flag for 36 h. The interactions between TSPAN4-Flag and Ub^{K48}-HA were analyzed via co-immunoprecipitation assay ($n = 3$ independent experiments). Source data are provided as a Source Data file. **k** HEK293T cells were transfected with Ub^{K48}-HA and TSPAN4-Flag, with OGT-Myc or OGT^{K852M}-Myc for 36 h. The interactions between TSPAN4-Flag and Ub^{K48}-HA were analyzed via co-immunoprecipitation assay ($n = 3$ independent experiments). Source data are provided as a Source Data file.

modulate viral release via migrasomes. AMFR has been reported to catalyze K27-linked polyubiquitination of STING upon microbial DNA challenge[33]. To exclude the effect of AMFR on viral release through the regulation of STING, we assayed the viral release in *Sting* KO cells, and found that overexpression of wild-type AMFR, but not AMFR^{3CS}, still inhibited viral release in *Sting* KO cells (Supplementary Fig. 4a, b). To confirm that AMFR regulates viral release dependent on TSPAN4, we gradually increased TSPAN4 expression and observed that the AMFR expression-induced reduction in viral release was reversed (Supplementary Fig. 4c). In *Tspan4* KO cells, AMFR overexpression had a minor effect on viral release (Supplementary Fig. 4d). To excluded the possibility that AMFR could theoretically suppress viral infection by degrading viral proteins, we co-expressed AMFR with VSV or HSV-1 proteins, and found that AMFR expression cased no effect on the protein level of viral proteins (Supplementary Fig. 4e). Additionally, overexpression of TSPAN4 still enhanced the viral release in *Amfr* KO cells, suggesting that the pro-viral function of TSPAN4 is not dependent on the antiviral effects of AMFR (Supplementary Fig. 4f). Thus, AMFR expression inhibits viral release through degrading TSPAN4.

Next, we sought to determine whether viral release is affected by the *O*-GlcNAcylation of AMFR. The reduction in viral release induced by AMFR expression was partially reversed by TMG treatment or overexpression of wild-type OGT (but not OGT^{K852M}), indicating that the *O*-GlcNAcylation of AMFR promotes viral release (Fig. 6a, b). We further conducted rescue experiments in OGT KD cells and found that expression of wild-type OGT, but not the OGT^{K852M} mutant, reversed the reduction of viral release (Fig. 6c). Together, these results indicate that OGT-mediated *O*-GlcNAcylation of AMFR enhances viral release by stabilizing TSPAN4.

Virus infection dynamically regulates AMFR *O*-GlcNAcylation and TSPAN4 ubiquitination

Given that both the migrasome formation and TSPAN4 stability were dynamically regulated at increasing time intervals following viral infection, we then investigated whether AMFR *O*-GlcNAcylation, TSPAN4 ubiquitination, and AMFR-TSPAN4 interactions are dynamically affected by viral infection. Based on the protein levels of TSPAN4, we set up the early stage of infection using 6 h post-infection (hpi) for VSV and 12 hpi for HSV-1 when TSPAN4 was upregulated. The late stage of infection using 12 hpi for VSV and 24 hpi for HSV-1, when TSPAN4 was downregulated (Fig. 1k, l). We first evaluated the K48-linked polyubiquitination levels of TSPAN4 in both mock and virus-infected cells. Consistent with the protein levels of TSPAN4 following virus infection, we observed that both VSV and HSV-1 infections decreased TSPAN4 ubiquitination at early stage of infection but increased TSPAN4 ubiquitination at late stage of infection (Fig. 6, e). Indeed, virus infections enhanced AMFR-OGT interactions and AMFR *O*-GlcNAcylation at the early stage, followed by a decrease at the late stage (Fig. 6f–i). Additionally, AMFR-TSPAN4 interactions were also downregulated at the early stage of infection and slightly upregulated at the late stage of infection (Fig. 6j, k). These results suggest that virus infection dynamically regulates AMFR *O*-GlcNAcylation and subsequently AMFR-mediated TSPAN4 ubiquitination.

Next, we sought to determine why AMFR *O*-GlcNAcylation is reduced during the late stages of viral infection. High-glucose conditions are known to promote *O*-GlcNAcylation. Intracellular glucose levels were measured and showed a significant decrease during the late stages of viral infection (Supplementary Fig. 4g), indicating that viral infection reduces intracellular glucose levels, thereby contributing to the reduction in AMFR *O*-GlcNAcylation. Interestingly, compare to mock cells, there was no significant increase of glucose level during the early stages of infection (Supplementary Fig. 4g), indicating that the upregulated AMFR *O*-GlcNAcylation during the early stages of infection is not caused by increased glucose level, and AMFR may undergo additional post-translational modifications that contribute to its enhanced *O*-GlcNAcylation.

We then investigated whether glucose regulate migrasome formation and subsequent viral release. TSPAN4-mCherry-NRK cells were cultured in DMEM medium containing varying glucose concentrations. Compared to the 25 mM glucose condition, low glucose (5.5 mM) decreased migrasome formation and viral release, whereas high glucose (50 mM) slightly enhanced these processes (Supplementary Fig. 4h, i). These findings suggest that during the early stages of infection, elevated glucose levels promote AMFR *O*-GlcNAcylation and subsequent migrasome formation to facilitate viral release, while during the late stages, viral infection leads to diminished intracellular glucose levels, resulting in reduced AMFR *O*-GlcNAcylation and impaired migrasome formation.

Virus infection regulates migrasome formation via AMFR-TSPAN4 axis

We then determine whether virus infection dynamically regulate migrasome formation by modulating AMFR *O*-GlcNAcylation and TSPAN4 ubiquitination. Our findings indicate that at the early stage of infection, VSV or HSV-1 failed to enhance the protein levels of TSPAN4 or promote migrasome formation in OGT knockdown cells, suggesting

https://doi.org/10.1038/s41467-025-68220-3

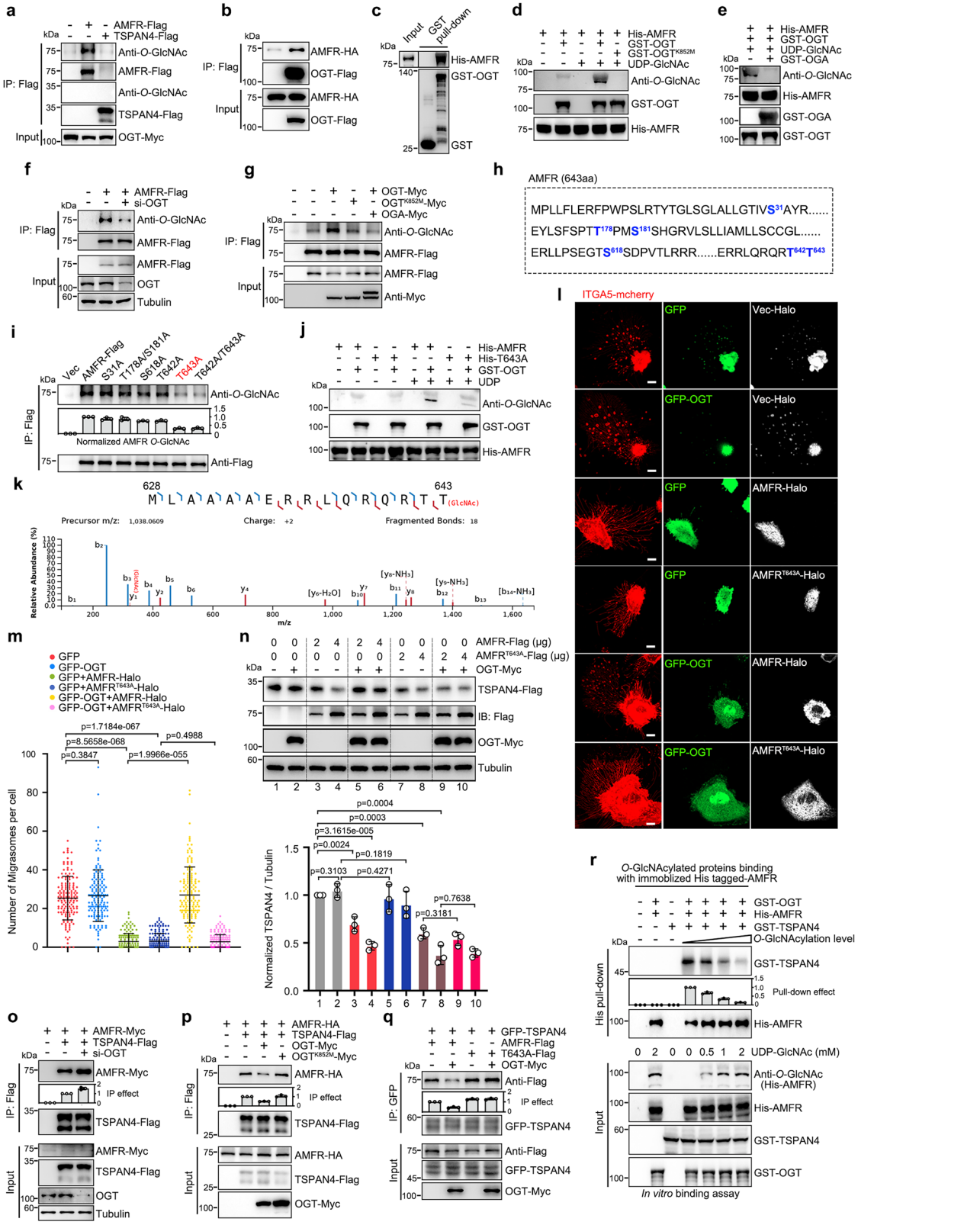

that during the early stage of infection viral infection enhances migrasome formation by upregulating AMFR *O*-GlcNAcylation (Supplementary Fig. 5a–d).

At the late stage of infection, TSPAN4 exhibited greater stability in *Amfr* KO cells compared to wild-type cells, and virus infection failed to impair migrasome formation in *Amfr* KO cells (Fig. 7a–c and Supplementary Fig. 5e, f). Wild-type AMFR (but not AMFR^{3CS}) effectively rescued viral infection-induced TSPAN4 degradation and the inhibition of migrasome formation in *Amfr* KO cells (Fig. 7d–f and Supplementary Fig. 5g, h). TSPAN4^{6KR} mutant demonstrated increased stability compared to the wild-type during viral infection, and viral infection did not hinder TSPAN4^{6KR}-mediated migrasome formation (Fig. 7g–i and Supplementary Fig. 5i, j). Notably, overexpression of OGT, but not OGT^{K852M}, counteracted the degradation of TSPAN4 and

Fig. 5 | *O*-GlcNAcylation of AMFR impairs AMFR-TSPAN4 interactions. **a** HEK293T cells were transfected with AMFR-Flag or TSPAN4-Flag and OGT-Myc. Flag antibody immunoprecipitated or cell lysates were subjected to WB ($n = 3$ independent experiments). *O*-GlcNAc antibody RL2 was used. Source data are provided as a Source Data file. **b** Co-immunoprecipitation assay for the interactions between AMFR-HA and OGT-Flag in HEK293T cells ($n = 3$ independent experiments). Source data are provided as a Source Data file. **c** GST pull-down analysis of GST-OGT with His-AMFR ($n = 3$ independent experiments). Source data are provided as a Source Data file. **d** OGT directly *O*-GlcNAcylates AMFR in vitro. In vitro glycosylation assay was performed with His-AMFR as substrate, which was incubated with purified GST-OGT, and the GlcNAcylated AMFR was blotted with RL2 antibody and the total His-AMFR and purified GST-OGT proteins were detected by WB ($n = 3$ independent experiments). Source data are provided as a Source Data file. **e** AMFR *O*-GlcNAcylation is reversed by OGA via in vitro glycosylation assay ($n = 3$ independent experiments). Source data are provided as a Source Data file. **f** HEK293T cells were transfected with or without OGT siRNA for 12 h, and cells were further transfected with AMFR-Flag for 36 h. Cell lysates were subjected to immunoprecipitation with Flag antibody and analyzed via WB ($n = 3$ independent experiments). Source data are provided as a Source Data file. **g** HEK293T cells were transfected with plasmids as indicated. Cell lysates were subjected to immunoprecipitation with Flag antibody and analyzed via WB ($n = 3$ independent experiments). Source data are provided as a Source Data file. **h** Diagram showing the amino acid sequence of AMFR and six potential *O*-GlcNAcylated sites. **i** HEK293T cells were transfected with indicated plasmids, and AMFR *O*-GlcNAcylation was analyzed by immunoprecipitation with Flag antibody and WB with the indicated antibodies. Quantification signal of AMFR and its mutants *O*-GlcNAcylation of immunoprecipitation from three independent experiments. Error bars represent the mean ± SD. Source data are provided as a Source Data file. **j** Purified WT or His-AMFR^{T643A} was used as substrates for in vitro glycosylation assay ($n = 3$ independent experiments). Source data are provided as a Source Data file. **k** LC-MS/MS spectrum of the *O*-GlcNAcylated peptide of AMFR. The Y1 ions confirm that *O*-GlcNAcylation occurs at T643. **l**, **m** NRK-ITGA5-mCherry cells were transfected with indicated plasmid. Cells were imaged by confocal microscopy. Green, GFP and OGT-GFP; red, ITGA5-mCherry; white, Halo, AMFR-Halo and AMFR^{T643A}-Halo. Number of migrasomes from the cells in (**l**); $n = 150$ cells per group from three independent experiments. Scar bar represents 10 μm. Error bars, mean ± SD. Two-tailed Unpaired Student's *t*-test. Source data are provided as a Source Data file. **n** HeLa cells stably expressing TSPAN4-Flag were transfected with indicated plasmids for 24 h. Lysates were analyzed via WB. Relative intensity of TSPAN4 of three independent experiments normalized to Tubulin, was quantified. Error bars, mean ± SD. Two-tailed Unpaired Student's *t*-test. Source data are provided as a Source Data file. **o** HEK293T cells were transfected with or without OGT siRNA for 12 h, and cells were further transfected with AMFR-Myc and TSPAN4-Flag for 36 h. Cell lysates were subjected to immunoprecipitation with Flag antibody and analyzed via WB. Quantification signal of AMFR-Myc of co-immunoprecipitation from three independent experiments. Error bars represent the mean ± SD. Source data are provided as a Source Data file. **p** HEK293T cells were transfected with the indicated plasmids for 36 h. Cell lysates were subjected to immunoprecipitation with Flag antibody and analyzed via WB. Quantification signal of AMFR-HA of co-immunoprecipitation from three independent experiments. Error bars represent the mean ± SD. Source data are provided as a Source Data file. **q** HEK293T cells were transfected with the indicated plasmids for 36 h. Cell lysates were subjected to immunoprecipitation with GFP antibody and analyzed via WB. Quantification signal of AMFR-Flag and its mutant of co-immunoprecipitation from three independent experiments. Error bars represent the mean ± SD. Source data are provided as a Source Data file. **r** *O*-GlcNAcylation of AMFR decrease AMFR-TSPAN4 interactions in vitro. His-AMFR was first incubated with OGT and UDP-GlcNAc for 4 h, then incubated with GST-tagged TSPAN4. Immunoprecipitation was performed with anti-His antibody. Quantification signal of GST-TSPAN4 of Pull-down from three independent experiments. Error bars represent the mean ± SD. Source data are provided as a Source Data file.

the inhibition of migrasome formation induced by viral infection (Fig. 7j–l and Supplementary Fig. 5k, l).

Together, these data indicated that during the early stage of infection, viruses enhanced AMFR *O*-GlcNAcylation, which resulted in the reduction of TSPAN4 ubiquitination and the increased migrasome formation to facilitate viral release. Conversely, at the late stage of infection, AMFR *O*-GlcNAcylation was downregulated, leading to an increase in TSPAN4 ubiquitination. Consequently, the degradation of TSPAN4 in infected cells inhibited migrasome formation.

Disscusion

Here, we propose an intriguing mechanism whereby, during the early stage of infection, only a small amount of progeny viruses is produced with limited transmission capacity. To facilitate efficient dissemination while evading immune detection, viruses preferentially exploit migrasomes for intercellular spread. This process is mediated by enhanced *O*-GlcNAcylation of AMFR, which inhibits AMFR-dependent degradation of TSPAN4, thereby promoting migrasome formation. In contrast, during the late stages of infection, when substantial quantities of progeny viruses are produced, migrasome-mediated transmission becomes inadequate to accommodate the heightened demand for viral release, thereby shifting from facilitating to impeding viral dissemination. Consequently, viruses downregulate migrasome formation by reducing AMFR *O*-GlcNAcylation and enhancing AMFR-mediated TSPAN4 degradation (Fig. 7m).

So far, migrasomes exhibit three modes of main functions: delivering signaling molecules, facilitating lateral transfer of mRNA or proteins, and disposing damaged mitochondria[34]. Several characteristics make migrasomes a potential tool for mediating viral release: (1) the most significant function of migrasomes is their ability to act as delivery packets, migrasomes generated by one cell can be engulfed by another, which make migrasomes highly effective transport vehicles for the lateral transfer of materials among surrounding cells; (2) migrasomes have been shown to be enriched with cholesterol[16], a major component of plasma membrane lipid rafts that is crucial for the budding of enveloped viruses; (3) the diameter of migrasomes is approximately 2 μm, which is considerably larger than the diameter of most viruses (approximately 10–300 nm). Previous studies have suggested that migrasomes may play a role in virus replication. For instance, HSV-2 virions were encapsulated in migrasomes, and Chikungunya virus (CHIKV) infection induces migrasome formation[9,11]. However, the mechanisms by which viruses regulate migrasome formation and utilize migrasomes for viral release remain to be elucidated. Here, we found that viruses such as VSV and HSV-1 also enriched in migrasomes, and these viral particles are infectious and use migrasome to spread among surrounding cells. More intriguingly, we found that migrasome formation can be dynamically regulated during viral infection. Viruses initially prefer to use migrasomes for release during the early stages of infection, but later migrasome-mediated viral spread would not suffice to accommodate the substantial release of viruses. This phenomenon may explain why viruses initially promote but subsequently inhibit migrasome formation. Alternatively, another possible explanation is that infected cells exploit the strategy of AMFR-mediated TSPAN4 degradation, which subsequently inhibits migrasome formation to reduce viral release. Nevertheless, our data support the concept that virions are enriched in TSPAN4-mediated migrasomes, suggesting that migrasomes serve as a novel strategy for viral release. Further evidence is required to investigate the potential mechanisms by which viral particles traffic to migrasomes.

TSPAN4 belongs to the tetraspanin family, which has 33 members and all of them contain four transmembrane domains[14]. TSPAN4 is first identified as a marker for migrasomes, and later found that its gain and loss results in an increase and fall in the formation of migrasomes[16]. However, the regulatory mechanisms governing TSPAN4 remain unknown. TSPAN4 molecules migrate toward and accumulate on local membrane swellings on the RFs, where increased membrane tension drives initial migrasome budding, indicating that TSPAN4 enrichment is essential for migrasome growth and stabilization[35,36]. Additionally, by

https://doi.org/10.1038/s41467-025-68220-3

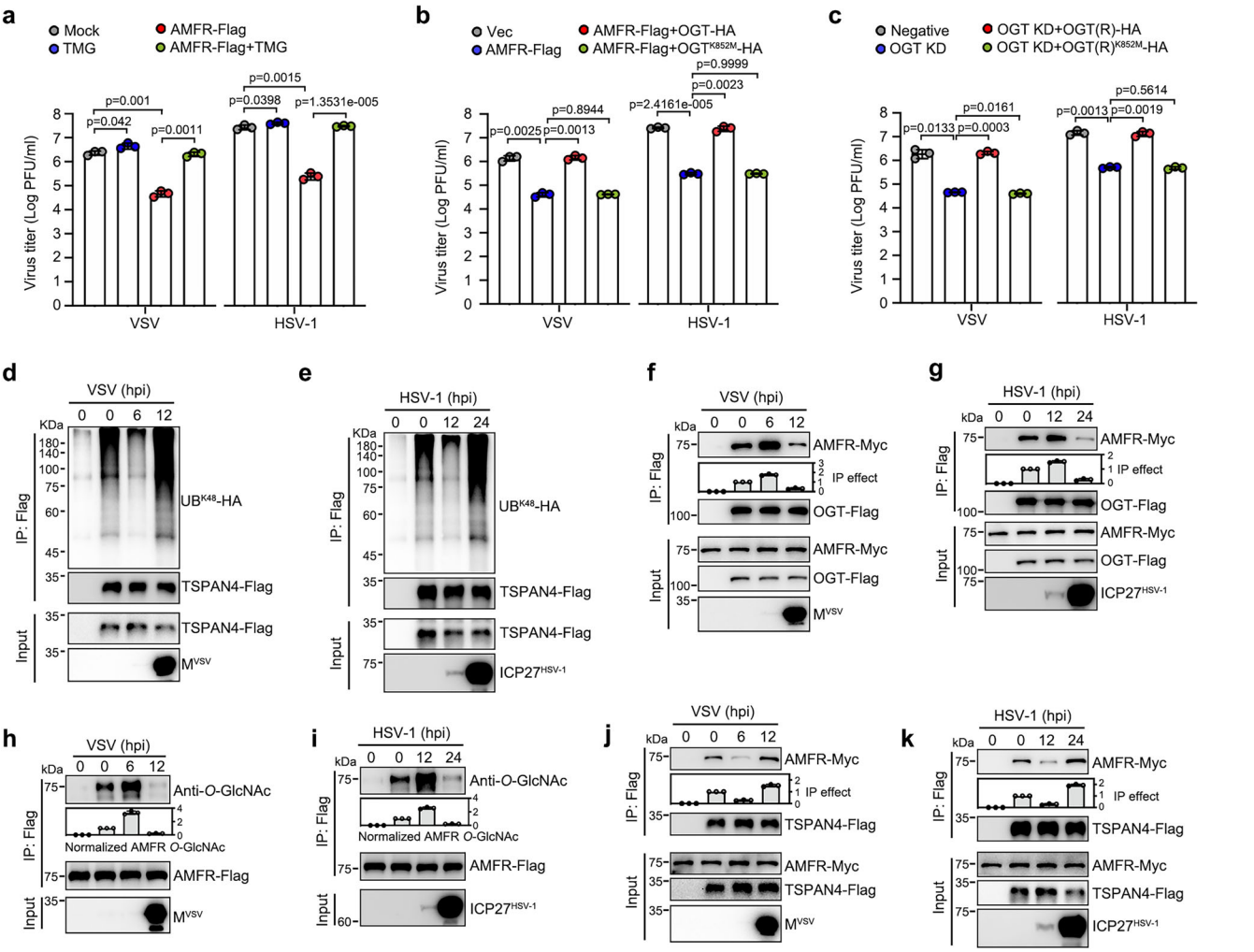

Fig. 6 | Viruses dynamically regulate AMFR *O*-GlcNAcylation and TSPAN4 ubiquitination. a NRK cells stably expressing TSPAN4-Flag were transfected with or without AMFR-Flag and infected with VSV-GFP (MOI = 0.01) or HSV-1 (MOI = 0.01) for 12 or 36 h and treated with or without 10 μM TMG for 6 h. Culture supernatants were collected, and viral titers were quantified using plaque assays. Data represent the mean ± SD from three biological replicates. Statistical significance was determined using a two-tailed Student's *t*-test. Source data are provided as a Source Data file. **b** NRK cells stably expressing TSPAN4-Flag were transfected with or without AMFR-Flag, OGT-HA, or OGT^{K852M}-HA and infected with VSV-GFP (MOI = 0.01) or HSV-1 (MOI = 0.01) for 12 or 36 h. Culture supernatants were collected, and viral titers were quantified using plaque assays. Data represent the mean ± SD from three biological replicates. Statistical significance was determined using a two-tailed Student's *t*-test. Source data are provided as a Source Data file. **c** WT and OGT KD NRK cells stably expressing TSPAN4-Flag were transfected with or without OGT(R)-HA, or OGT(R)^{K852M}-HA and infected with VSV-GFP (MOI = 0.01) or HSV-1 (MOI = 0.01) for 12 or 36 h. Culture supernatants were collected, and viral titers were quantified using plaque assays. Data represent the mean ± SD from three biological replicates. Statistical significance was determined using a two-tailed Student's *t*-test. Source data are provided as a Source Data file. **d**, **e** Analysis of interactions between TSPAN-Flag and HA-Ub^{K48} under VSV-GFP or HSV-1 infection at an MOI of 1 for indicated time by co-immunoprecipitation assay ($n = 3$ independent experiments). Source data are provided as a Source Data file. **f**, **g** Analysis of interaction between AMFR-Myc and OGT-Flag with VSV-GFP or HSV-1 infection at an MOI of 1 for indicated time by co-immunoprecipitation assay. Quantification signal of AMFR-Myc of co-immunoprecipitation from three independent experiments. Error bars represent the mean ± SD. Source data are provided as a Source Data file. **h**, **i** Analysis the AMFR *O*-GlcNAcylation with VSV-GFP or HSV-1 infection at an MOI of 1 for indicated time by immunoprecipitation assay and analyzed by WB using anti-*O*-GlcNAc antibody. Quantification signal of AMFR *O*-GlcNAcylation of immunoprecipitation from three independent experiments. Error bars represent the mean ± SD. Source data are provided as a Source Data file. **j**, **k** Analysis of interaction between AMFR-Myc and TSPAN4-Flag with VSV-GFP or HSV-1 infection at an MOI of 1 for indicated time by co-immunoprecipitation assay. Quantification signal of AMFR-Myc of co-immunoprecipitation from three independent experiments. Error bars represent the mean ± SD. Source data are provided as a Source Data file.

mediating the assembly of Tetraspanin-enriched membrane microdomains (TEMs), cholesterol-enriched membrane domains that seal off the damage site to prevent it from expanding and thereby facilitate membrane repair, Tspan4 helps shield cells from membrane damage-induced cell death[37]. Here, our data highlight the important roles of TSPAN4 on viral release, and its gain and loss results in an increase and fall in the virus production. After 30 min of CHX treatment, we discovered that TSPAN4 was unstable and significantly deteriorated (Fig. 2a). According to reports, TSPAN4 can be found on the cytoplasmic membrane, endosomes, and migrasomes[16,17,38]. We found that TSPAN4 also partially colocalizes with ER and only ER-localized TSPAN4 is unstable and can be degraded upon AMFR overexpression, but not non-ER TSPAN4 (Fig. 3h). The degradation of ER-localized TSPAN4 induced by AMFR overexpression impaired migrasome formation. Our model predicted that ER-localized TSPAN4 may move to the cytoplasmic membrane by endosomes, where TSPAN4 was dynamically recruited to migrasomes via retraction fibres. Since ER-localized TSPAN4 might be the source of migrasome-localized TSPAN4, this could help to explain why the degradation of ER-localized TSPAN4 caused the defect of migrasome formation. Besides, we

https://doi.org/10.1038/s41467-025-68220-3

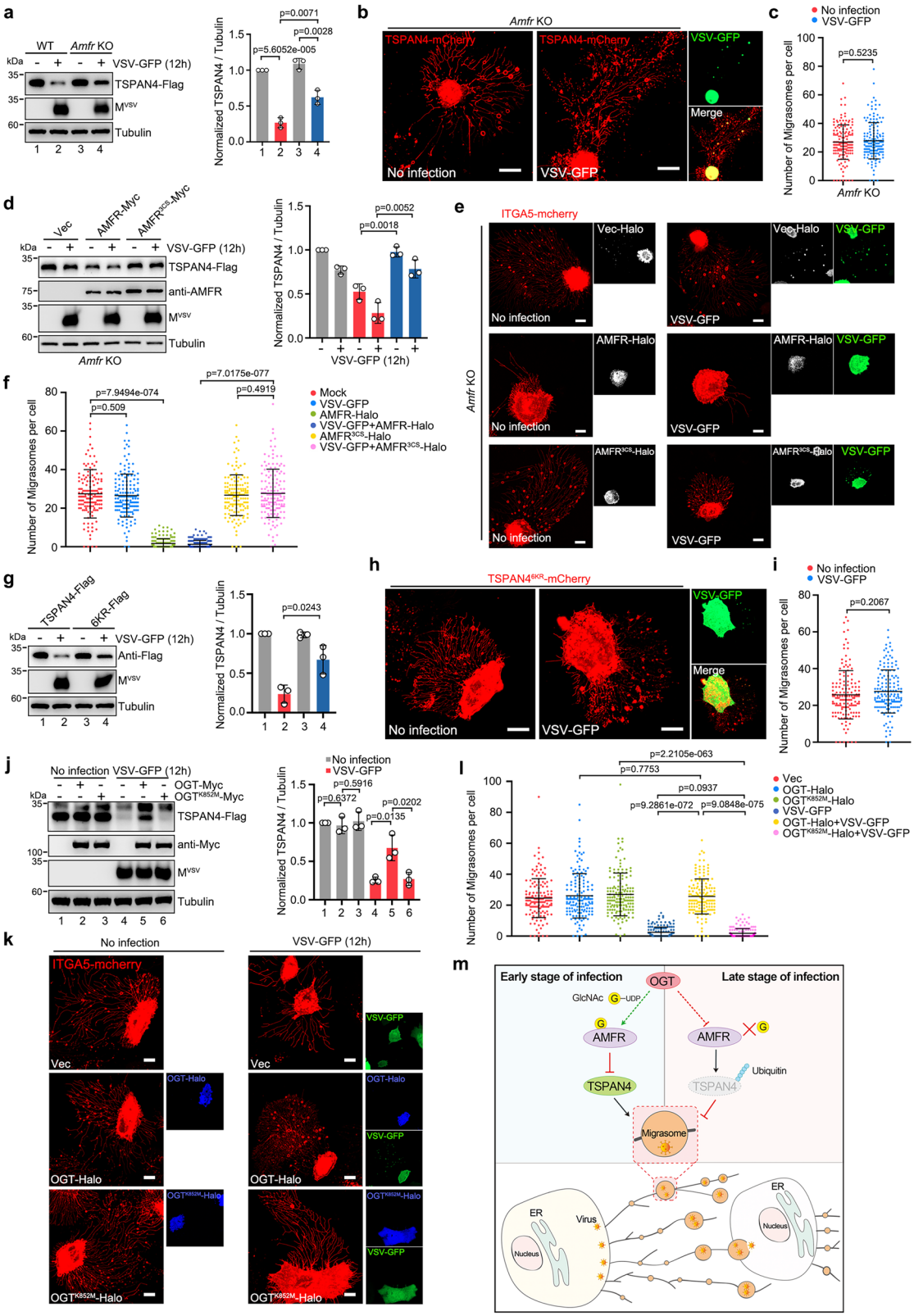

noticed that TSPAN4^{6KR} is still degraded, TSPAN4 degradation persists even when AMFR is knocked out, and more importantly, virus infection or AMFR expression-induced TSPAN4 degradation can also be partly inhibited upon CQ treatment. These results indicate that autophagosome-lysosome pathway may also be involved in TSPAN4 degradation. Additionally, TSPAN4 may undergo other post-translational modifications that could be relevant to its function in viral infection, and more evidences are required to investigate the potential mechanism(s) by which TSPAN4 regulate migrasome formation and viral release.

AMFR, a RING finger-dependent ubiquitin protein ligase of ER, was originally identified as the AMFR that drives tumor metastasis[30,39,40]. Numerous research conducted in recent years have demonstrated the diverse cellular physiological roles of AMFR in innate immune

Fig. 7 | Viruses regulate migrasome formation via AMFR-TSPAN4 axis. a *Amfr* WT and KO HeLa cells stably expressing TSPAN4-Flag were infected with or without VSV-GFP at an MOI of 1 for 12 h. Lysates were analyzed via WB. Relative intensity of TSPAN4 of three independent experiments normalized to Tubulin, was quantified. Error bars, mean ± SD. Two-tailed Unpaired Student's *t*-test. Source data are provided as a Source Data file. **b**, **c** *Amfr* KO NRK cells stably expressing TSPAN4-mCherry were infected with or without VSV-GFP at an MOI of 0.2 for 12 h. Cells were imaged by confocal microscopy. Green, VSV-GFP; red, TSPAN4-mCherry; yellow, Merge. Number of migrasomes from the cells in (**b**); $n = 150$ cells per group from three independent experiments. Scar bar represents 10 μm. Error bars, mean ± SD. Two-tailed Unpaired Student's *t*-test. Source data are provided as a Source Data file. **d** *Amfr* KO HeLa cells stably expressing TSPAN4-Flag were transfected with or without AMFR-Myc or AMFR^{3CS}-Myc for 24 h and then infected with VSV-GFP at an MOI of 1 for another 12 h. Lysates were analyzed via WB. Relative intensity of TSPAN4 of three independent experiments normalized to Tubulin, was quantified. Error bars, mean ± SD. Two-tailed Unpaired Student's *t*-test. Source data are provided as a Source Data file. **e**, **f** *Amfr* KO NRK cells stably expressing ITGA5-mCherry with or without AMFR-Halo or AMFR^{3CS}-Halo were infected with VSV-GFP at an MOI of 0.2 for 12 h. Cells were imaged by confocal microscopy. Green, VSV-GFP; red, ITGA5-mCherry; white, Halo, AMFR-Halo, and AMFR^{3CS}-Halo. Number of migrasomes from the cells in (**e**); $n = 150$ cells per group from three independent experiments. Scar bar represents 10 μm. Error bars, mean ± SD. Two-tailed Unpaired Student's *t*-test. Source data are provided as a Source Data file. **g** HeLa cells stably expressing TSPAN4-Flag or TSPAN4^{6KR}-Flag were infected with or without VSV-GFP at an MOI of 1 for 12 h. Lysates were analyzed via WB. Relative intensity of TSPAN4 of three independent experiments normalized to Tubulin was quantified. Error bars, mean ± SD. Two-tailed Unpaired Student's *t*-test. Source data are provided as a Source Data file. **h**, **i** NRK cells stably expressing TSPAN4^{6KR}-mCherry were infected with or without VSV-GFP at an MOI of 0.2 for 12 h. Green, VSV-GFP; red, TSPAN46^{KR}-mCherry; yellow, Merge. Cells were imaged by confocal microscopy. Number of migrasomes from (**h**); $n = 149$ no infection, $n = 149$ VSV-GFP from three independent experiments. Scar bar represents 10 μm. Error bars, mean ± SD. Two-tailed Unpaired Student's *t*-test. Source data are provided as a Source Data file. **j** HeLa cells stably expressing TSPAN4-Flag were transfected with or without OGT-Myc or OGT^{K852M}-Myc for 24 h and then infected with or without VSV-GFP at an MOI of 1 for another 12 h. Lysates were analyzed via WB. Relative intensity of TSPAN4 of three independent experiments normalized to Tubulin, was quantified. Error bars, mean ± SD. Two-tailed Unpaired Student's *t*-test. Source data are provided as a Source Data file. **k**, **l** NRK cells stably expressing ITGA5-mCherry transfected with or without OGT-Halo or OGT^{K852M}-Halo were infected with or without VSV-GFP at an MOI of 0.2 for 12 h. Cells were imaged by confocal microscopy. Green, VSV-GFP; red, ITGA5-mCherry; blue, OGT-Halo and OGT^{K852M}-Halo. Number of migrasomes from the cells in (**k**); $n = 150$ cells per group from three independent experiments. Scar bar represents 10 μm. Error bars, mean ± SD. Two-tailed Unpaired Student's *t*-test. Source data are provided as a Source Data file. **m** Proposed model for virus infection dynamically regulates migrasome formation via AMFR *O*-GlcNAcylation and TSPAN4 ubiquitination.

response[33], inflammation[41], mitophagy[42], ER-phagy[43], metabolism[44], and so forth. The roles that AMFR plays in antiviral effects are already indicated: AMFR promotes proteasomal degradation of HMGCR, the rate-limiting enzyme of the cholesterol biosynthesis pathway in response to influenza virus infection[45]; knockdown of AMFR results in a corresponding enhancement of MAVS signaling[46]; HIV p6 protein negatively regulates K27-linked STING ubiquitination mediated by AMFR to suppress IFN-I and promote immune evasion[33,47]. Thus far, limited knowledge exists on the role of AMFR and its potential function as an E3 ligase in the regulation of migrasome-mediated viral release. We showed here that AMFR modulates viral release through migrasomes, which is independent on immune response. AMFR mediates the K48-linked TSPAN4 ubiquitination for degradation, and only the ER-localized TSPAN4 can be ubiquitinated and degraded by AMFR. Although the protein level of AMFR remain unchanged upon virus infection, the AMFR-TSPAN4 interactions are dynamically regulated during virus replication. The decreased AMFR-TSPAN4 interaction during early infection stage led to the accumulation of TSPAN4 and increased migrasome formation for viral release. While the enhanced AMFR-TSPAN4 interaction during late infection stage resulted in the degradation of TSPAN4 and the suppression of migrasomes. of AMFR depletion at late infection stage abolished virus-induced degradation of TSPAN4 and migrasome inhibition. Furthermore, we found that AMFR-TSPAN4 interaction was regulated by OGT-mediated *O*-GlcNAcylation. *O*-GlcNAcylated-AMFR showed poorer interaction with TSPAN4. Based on the predicted structure of AMFR-TSPAN4 complex from AlphaFold, the potential *O*-GlcNAcylation site T643 is near the AMFR-TSPAN4 interaction regions, indicating that *O*-GlcNAcylation modification of T643 induce steric effects on the interaction interface. Further structural analyses of the AMFR and *O*-GlcNAcylated AMFR should be carried out to investigate the details of the mechanisms by which *O*-GlcNAcylation regulate the AMFR-TSPAN4 interactions.

Overall, our study presents a compelling mechanism by which viruses dynamically regulate the formation of migrasomes through modulation of TSPAN4 stability. Furthermore, migrasomes may serve as a potential tool for facilitating viral release among neighboring cells. We also elucidate the role of AMFR as an E3 ligase responsible for the ubiquitination and subsequent degradation of TSPAN4, with the interaction between AMFR and TSPAN4 being regulated by OGT-mediated *O*-GlcNAcylation on AMFR. This research highlights the significant roles that migrasomes play in viral release and proposes potential strategies to impede viral dissemination by targeting the AMFR-TSPAN4 axis that governs migrasome formation.

Methods

Cell culture

HEK293T cells (CRL-1573) and HeLa cells (CCL-2) were obtained from ATCC. BHK21 cells were obtained from Mingzhou Chen (Wuhan University). Vero-E6 cells were obtained from Kun Cai (Hubei Provincial Center for Disease Control and Prevention). L929 TSPAN4-mCherry cells, NRK cells, and L929 ITGA5-GFP cells were obtained from Li Yu (Tsinghua University). *TSPAN4* WT and KO HeLa, *AMFR* WT and KO HeLa, *Tspan4* WT and KO NRK, *Amfr* WT and KO NRK, TSPAN4-mCherry NRK, TSPAN4-GFP NRK, TSPAN46^{KR}-mCherry NRK, ITGA5-mCherry NRK, TSPAN4-Flag NRK, and TSPAN4-Flag L929 cells were constructed in our lab. All cells were cultured in Dulbecco's Modified Eagle's Medium (DMEM) (Gibco, 11995065) supplemented with 10% Fetal Bovine Serum (FBS) (Sigma-Aldrich, 12303 C) and 1% penicillin-streptomycin (Gibco, 15140163) at 37 °C in 5% CO_2. All cells were tested for mycoplasma negative.

Antibodies and reagents

Mouse anti-Flag (AE005, western blot (WB) 1:5000), mouse anti-HA (AE008, WB 1:5000), rabbit anti-Myc (AE070, WB 1:10000), mouse anti-GFP (AE012, WB 1:5000), mouse anti-GST (AE001, WB 1:5000), and mouse anti-His (AE003, WB 1:5000) were obtained from ABclonal. Rabbit anti-HA (3724, WB 1:1000), rabbit anti-Rab11 (5589, WB 1:2000), and rabbit anti-Integrin α5 (4705, WB 1:1000) were obtained from Cell Signaling Technology. Mouse anti-Tubulin (E7, WB 1:10000) was obtained from Developmental Studies Hybridoma Bank. Mouse anti-GAPDH (sc-365062, WB 1:5000), mouse anti-HSV-1/2 ICP27 (SC-69807, WB 1:500), mouse anti-VSV-G (SC-365019, WB 1:500, IF 1:200) and mouse anti-TOM20 (SC-17764, WB 1:500) were obtained from Santa Cruz Biotechnology. Mouse anti-VSV-M (EB0011, WB 1:1000) was obtained from Kerafast. Rabbit anti-HSV-1/2 (PA1-7214, IF 1:2000) was obtained from ThermoFisher Scientific. Mouse anti-O-Linked N-Acetylglucosamine (RL2) antibody (ab2739, WB 1:1000), Rabbit anti-PIGK antibody (ab201693, WB 1:2000), Rabbit anti-Calnexin antibody (ab22595, WB 1:800), and Rabbit anti-EOGT antibody (ab190693, WB 1:5000) were obtained from Abcam. Rabbit anti-AMFR (16675-1-AP, WB 1:5000) and Mouse anti-HSP90 (60318-1-Ig, WB 1:10000) were obtained from Proteintech. HRP-conjugated goat anti-mouse IgG

(H + L) (AS003, WB 1:10000), HRP-conjugated goat anti-rabbit IgG (H + L) (AS014, WB 1:10000), and HRP-conjugated goat anti-mouse IgG heavy chain (AS064, WB 1:10000) were obtained from Abclonal. Peroxidase-AffiniPure goat anti-mouse IgG light-chain-specific (115-035-174, WB 1:10000) was obtained from Jackson Immunoresearch. Alexa Fluor 568-conjugated goat anti-mouse IgG (H + L) (A-11031, IF 1:500) and goat anti-rabbit IgG (H + L) (A-11036, IF 1:500) were purchased from Thermo Fisher Scientific.

Plasmid construction

shCert, shCers5, shSgms2, sgTSPAN4, sgRab35, sgPIP5K1A, GFP tagged TSPAN4, and ITGA5 were provided by Li Yu (Tsinghua University). mCherry-TSPAN1, mCherry-TSPAN2, pmCherry-TSPAN8, and mCherry-TSPAN9 were provided by Yuwei Huang (Xian Jiaotong University). OGA-Myc was provided by Lidong Sun (Huazhong University of Science and Technology). GST tagged full length OGT was a gift from Hong Zhang (Chinese Academy of Sciences). VSV-N-Myc and VSV-G-Myc were provided by Mingzhou Chen (Hubei University). HSV-1-UL17-Flag, HSV-1-UL5-Flag, and HSV-1-ICP4-Flag were provided by Yujie Ren (Wuhan Institute of Virology) and Junjie Zhang (Wuhan University). pCDNA4-ICP27-strep was cloned into pCDNA4-strep vector. pCDNA4-VSV-M-HA was cloned into pCDNA4-HA vector. cDNA encoding human and mouse-AMFR and its point mutants were respectively cloned into pCDNA4 vector with a HA, Flag, or Myc tag, or pCOLD-6 × His-sumo vector. pLenti-mCherry-Ramp4 was cloned into the mammalian expression vector pLenti-N1-mCherry. pLenti-mTSPAN4-Flag and its mutants were cloned into pLenti-Flag vector. pLenti-hTSPAN4-Flag was cloned into pLenti-Flag vector. pLenti-mAMFR-Flag and its mutants were cloned into pLenti-Flag vector. pLenti-TSPAN4-GFP was cloned into pLenti-GFP vector. pLenti-ITGA5-mCherry was cloned into pLenti-mCherry vector. pLenti-AMFR-GFP and its point mutants were cloned into pLenti-GFP vector. pLenti-OGT-GFP and its point mutant was cloned into pLenti-GFP vector. pLenti-AMFR-Halo and its point mutants were cloned into pLenti-Halo vector. pLenti-OGT-Halo and its point mutants were cloned into pLenti-Halo vector. pCDNA3.0-HA-UB, pCDNA3.0-HA-UB^{K48}, and pCDNA3.0-HA-UB^{K63} were cloned into the mammalian expression vector pCDNA3.0-HA. GST-OGA (31-624), GST-TSPAN4, GST-OGT (323-1041), and its point mutant were cloned into pGEX-2T vector. Full length OGT and its point mutant were cloned into pCDNA4 vector with a HA, Flag, or Myc tag. All mutant constructs in this study were introduced by using a PCR-mediated site-directed mutagenesis on the basis of their respective wild-type constructs. All constructs were confirmed by sequencing.

DNA transfection and RNA interference

Plasmid DNAs were transfected into HEK293T cells using Polyethylenimine Linear (Yeasen, 40815ES03). siRNA oligonucleotides were purchased from GenePharma. siRNAs were transfected into cells with iboFECT CP Transfection Kit (RiboBio, C10511-05). Cells were harvested 48 h after transfection, the efficiency of protein knockdown was determined by Western blot analysis. siRNA targeting sequences for OGT: GAUUAAGCCUGUUGAAGUCTT, siRNA targeting sequences for TRIM21: AGAUUCUUGAGCAGAAAGCGC. siRNA targeting sequences for UBA1: UGAAAAGGAGACAAAGUCCCC. siRNA targeting sequences for AMFR: AAAAUUUGUCUUUGAGAUGCU. siRNA targeting sequences for UBQLN4: UCGGCCCCGCUCGGCUCCGCC. siRNA targeting sequences for UBQLN2: UUUUUCCGGCAAAAAUCAGCA. siRNA targeting sequences for LTN1: UUGAAUAGCAGGAACAUAGCC.

CRISPR/Cas9 knockout

Single guide RNAs (sgRNAs) were produced using Synthego (https://www.synthego.com/products/bioinformatics/crispr-design-tool), and annealed and ligated into BsmBI-cut pLenti-CRISPR-V2 vectors. The plasmid was transfected together with pMD2.G and psPAX2 into HEK293T cells to produce recombinant lentivirus. The supernatant from transfected HEK293T cells were filtered through a syringe with 0.22 μm filters. Cells were infected with Lentivirus for 24 h, and then selected with puromycin. sgRNA targeting for mouse-AMFR #1: AAGCGCTCGAGGAAGAGCAG. mouse-AMFR #2: TGAGGCCCGTGTAGGTGCGG. sgRNA targeting sequences for mouse-STING #1: GCCGTGGGATGGCTGGATGC, mouse-STING #2: GTGACCTCTGGGCCGTGGGA, mouse-STING #3: AGCGGTGACCTCTGGGCCGT. sgRab35 and sgPIP5K1A were obtained from Li Yu (Tsinghua University).

In vivo *O*-GlcNAcylation assay

HEK293T cells were co-transfected with AMFR-Flag, OGT-Myc, and other plasmids, where indicated for 48 h. Cells were collected into TAP lysis buffer (20 mM Tris-HCl, pH 7.5, 150 mM NaCl, 0.5% NP-40, 1 mM EDTA, Protease cocktail) and lysed for 30 min on ice, and cleared by centrifugation at 13,000 rpm (16,060 × *g*) for 20 min at 4 °C. Cell lysate was incubated with anti-Flag magnetic beads (Bimake, B26102) by rotation at 4 °C for 6 h. Beads were then washed with TAP wash buffer (20 mM Tris-HCl, pH 7.5, 500 mM NaCl, 0.5% NP-40, 1 mM EDTA) for three times. Samples were then added 1× SDS protein loading buffer and analyzed by western blot with O-GlcNAc antibody (Abcam, ab2739).

In vitro *O*-GlcNAcylation assay

The purified wild-type His-AMFR or its mutants were incubated with recombinant and purified GST-OGT protein (323-1041) in 50 μL reactions buffer (50 mM Tris-HCl, 12.5 mM MgCl2, 1 mM DTT, 2 mM UDP-GlcNAc, pH 7.5) at 37 °C for 4 h. The samples were then added with 5× SDS protein loading buffer and detected by western blot with anti-*O*-GlcNAc (RL2) antibody (Abcam, ab2739).

OGA treatment assay

For *O*-GlcNAc cleavage, *O*-GlcNAcylated His-AMFR (OGT assay product) were treated with 5 μg purified OGA (31-624) at 37 °C for 2 h in a volume of 100 μl. Samples were then added 5× SDS protein loading buffer and analyzed by western blot with O-GlcNAc antibody (Abcam, ab2739).

Western blot

Cells were lysed by SDS lysis buffer (Beyotime Biotechnology, P0015L) and heated at 100 °C for 10 min. Equal amounts of protein were separated on 10% or 12% SDS-PAGE gels according to the molecular weight of target proteins, followed by electrophoretic transfer onto nitrocellulose membranes (Millipore, HATF00010). After blocking with 5% skim milk in PBST (135 mM NaCl, 4.7 mM KCl, 10 mM Na2HPO4, 2 mM NaH2PO4, 0.1% Tween-20) for 1 h at 37 °C, membranes were incubated with the relevant primary antibodies in the primary antibody dilution buffer (Absin, ABS954-1 L) overnight at 4 °C. After washing 3 times with PBST for 5 min each, the membranes were incubated with HRP-conjugated secondary antibodies in 1% skim milk for 1 h at 37 °C. Membranes were washed and signals were developed using ECL Plus western blot substrate (Biosharp, BL520B). Western blotting images were obtained using Tanon 5200 and analyzed using Bio-Rad Image Lab Software for PC Version 6.1.

Co-immunoprecipitation

HEK293T cells were transfected with indicated plasmids for 36 h, then cells were lysed in TAP lysis buffer (20 mM Tris-HCl, pH 7.5, 150 mM NaCl, 0.5% NP-40, 1 mM EDTA, Protease cocktail) for 30 min on ice. The lysates were centrifuged at 13,000 rpm (16,060 × *g*) for 20 min at 4 °C. For HA, Flag and GFP tag immunoprecipitation, tag magnetic beads were added in supernatants and incubated Ctogether with rotation at 4 °. Precipitated immunocomplexes were washed three times with TAP lysis buffer, five minutes each time. Finally, beads-bound proteins were added in 1 × SDS loading buffer and subjected to western blot. The

immunoprecipitated fractions were analyzed via mass spectrometry using 30 min LC-MSMS (Wuhan Genecreate Inc).

In vitro binding assay

His-tagged AMFR (WT, T643A, and S643A) was purified from *Escherichia coli*. The purified AMFR was subjected to in vitro *O*-GlcNAcylation assay for 4 h at 37 °C with different concentrations of UDP-GlcNAc to obtain different levels of *O*-GlcNAcylation. GST-tagged TSPAN4 proteins were obtained by immunoprecipitation with anti-GST affinity beads from *Escherichia coli* cells. The *O*-GlcNAcylated proteins were then incubated with GST-TSPAN4, in cytosolic buffer (40 mM HEPES pH 7.4, 0.1% Triton ×-100, 10 mM NaCl, 150 mM KCl, and 2.5 mM $MgCl_2$) by rotating at 4 °C for 2 h. The beads were then washed three times with Cytosolic Buffer and denatured by heating at 100 °C in 1× loading buffer for 10 min.

GST pull-down assay

His-fusion proteins or GST-fusion proteins were expressed in *Escherichia coli* strain BL21 (DE3). Then bacteria were grown at 37 °C until the OD value reached 0.6–0.8, the proteins expression were induced with 0.4 mM IPTG for 18 h at 16 °C. Bacteria were collected and lysed in lysis buffer (20 mM Tris, pH 7.4, 300 mM NaCl, 0.1% NP-40, 1 mM PMSF) by sonication on ice. Lysates were centrifuged at 12,000 × *g* for 20 min at 4 °C, and the supernatants mixed the indicated protein samples were incubated with corresponding agarose beads overnight at 4 °C. Then the beads were washed with lysis buffer and resuspended in 1× loading buffer, bound proteins were analyzed by western blot.

Cell imaging and image analysis

NRK cells were cultured in 35-mm confocal dishes (Biosharp, BS-20-GJM) pre-coated with 10 μg/ml fibronectin (Solarbio, F8180) in PBS for 3 h at 37 °C and grew for 12–15 h. Cells were stained with 5 nM Janilia Fluo 646 HaloTag Ligand for 30 min or 1 μg/ml WGA-Alexa 647 for 5 min at 37 °C. Images were acquired using Zeiss LSM 900 confocal microscopes.

To determine the cell migration speed, time-lapse images were acquired by Zeiss LSM 900, the interval was 2 min, and the duration was at least 4 h. For Time-lapse imaging of VSV-GFP-infected NRK cells stable expressing TSPAN4-mCherry. Cells were infected with VSV-GFP at an MOI of 0.2. Images were acquired using an Olympus FV-3000 (60×/1.30 silicone oil objective). Images were collected at 1024 × 1024 pixels resolution. The samples were maintained at 37 °C in an atmosphere containing 5% CO_2. The recording was set as every 6 min for 12 h, and one focal plane was recorded for all live-cell videos. Images were processed with ImageJ (RRID:SCR_003070), and statistical analyses were conducted using GraphPad Prism v9.5.1.

Immunostaining

Cells grown in 35 mm glass-bottom dishes were fixed with methanol for 5 min at −20 °C, washed 3 times with PBS and permeabilized with Saponin (Solarbio, P1070) in PBS for 5 min. Cells were then blocked with 5% BSA for 30 min at room temperature, and further incubated with the specific primary and secondary antibodies at room temperature in 5% BSA. After 3 washes with PBS. Images were acquired by Zeiss LSM 900 confocal microscopes.

Virus titration and viral plaque assays

Vero and BHK21 cells were seeded into 24-well plates, respectively one day prior. Next day, the cells were infected with tenfold diluted series of VSV-GFP and HSV-1 aliquots. Cells were incubated at 37 °C for 2 h. After infection, cells were replenished with a maintenance cover layer (DMEM with 2% FBS and 0.9% carboxy-methylcellulose). After 72 h incubation at 37 °C the plates were fixed with 4% paraformaldehyde overnight at 4 °C. Then the cells were stained with crystal violet for 15 min at room temperature and the viral plaque numbers were visualized. The viral titer in plaque-forming units (PFU) was then calculated according to the plaque number and dilution ratio.

The migrasomes produced by the VSV-GFP-infected cells from forty 150 mm dishes were isolated according to the method described in this study and suspended with 200 μl PBS. 15 μL of suspension-containing medium was serially diluted and then added to confluent Vero-E6 cells for viral plaque assays.

Attachment assay

NRK monolayers grown in 6-well plates were pre-chilled at 4 °C for 0.5 h and infected with VSV-GFP and HSV-1 at a MOI of 5 PFU/cell. Cells were incubated for 2 h at 4 °C and followed by three washes with cold PBS. The RNA was extracted and analyzed by real-time PCR to detect viral genomes.

Entry assay

For entry assays, NRK monolayers grown in 12-well plates were infected with VSV-GFP and HSV-1 at a MOI of 5 PFU/cell. Cells were incubated for 2 h at 4 °C and the unbound viruses were removed by washing with cold PBS. The cells were cultured with fresh medium supplemented with 10% FBS was added for 2 h at 37 °C. After a single wash with acidic glycine to remove virus particles from the cell surface, the RNA was extracted and analyzed by real-time PCR to detect viral genomes.

Detection of glucose concentrations

Glucose concentrations using a glucose detection kit (BestBio, BB-4731) according to the manufacturer's instructions. Briefly, cells were collected in cold PBS and centrifuged at 1000 × *g* for 5 min at 4 °C. The supernatant was removed then resuspended the cells in 200 μl lysis buffer and incubated for 30 min on ice. Lysates were centrifuged at 12,000 × *g* for 15 min at 4 °C and collected the supernatant. Then 10 μL of supernatant was added into the wells followed by the addition of 220 μL of the work solution and standard. After incubation at 37 °C for 15 min, the absorbance at 510 nm was measured.

Quantitative RT-PCR

Total RNA was extracted using TRIzol (Biosharp, BS259A). 1 μg of RNA was used for reverse-transcribed using Reverse Transcription Kit (Biosharp, BL699A) according to the manufacturer's protocol. The quantifications of cDNAs were performed by real-time PCR using qPCR Mix (Bio-Rad, 1725120). The PCR primers used as follows: hGAPDH forward 5′- GACAAGCTTCCCGTTCTCAG-3′, reverse 5′- GACAAGCTT CCCGTTCTCAG-3′; for Rat β-ACTIN forward 5′- GCGCAAGTACTCT GTGTGGA-3′, reverse 5′- AAGGGTGTAAAACGCAGCTC-3′; for VSV forward 5′-ACGGCGTACTTCCAGATGG-3′, reverse 5′- CTCGGTTCAAGAT CCAGGT-3′; for HSV-1 forward 5′- CATCACCGACCCGGAGAGGGAC-3′, reverse 5′- GGGCCAGGCGCTTGTTGGTGTA-3′.

For hIFN-β forward 5′-ATGACCAACAAGTGTCTCCTCC-3′, reverse 5′- GGAATCCAAGCAAGTTGTAGCTC-3′.

Generation of stable cell line

For generation of stable TSPAN4-Flag overexpressed HeLa cell line. The TSPAN4 coding sequence were cloned into pLenti-puro-Flag vector. Lentivirus were produced by co-transfecting pLenti-TSPAN4-Flag with packaging plasmids pMD2.G and psPAX2 into HEK293T cells. Forty-eight hours later, the supernatant from transfected HEK293T cells were collected and followed by filtering through a syringe with 0.22 μm filters. For HeLa cells were infected with Lentivirus for 48 h, puromycin (5 μg/ml) was added to select positive cells for two days. For the NRK cell lines with overexpression of GFP-tagged, mCherry-tagged, or Halo-tagged targets, L929 and NRK cell lines with overexpression of Flag-tagged targets were also constructed using the above method. For NRK and L929 cells were infected with Lentivirus for 48 h, puromycin (10 μg/ml) was added to select positive cells for

two days. The cell lines with stable overexpression were used for subsequent experiments.

Mass spectrometry for protein *O*-GlcNAcylation

AMFR peptide MLAAAAERRLQRQRTT (628-643) was synthesized (Zhuantai Biotech Inc., Anhui). In a protein *O*-GlcNAcylation experiment, 1.0 mg of peptide was dissolved in 100 µL of ddH_2O and prepared stock solution. Peptide stock solution was incubated with recombinant and purified GST-OGT protein (323-1041) in 50 µL reactions. Reaction buffer containing 50 mM Tris-HCl, 12.5 mM MgCl2, 1 mM DTT, 2 mM UDP-GlcNAc, pH 7.5) were incubated at 37 °C for 4 h and samples were conserved in liquid nitrogen. Samples analyzed via mass spectrometry using 60 min timsTOF Pro2 (Wuhan Baizhen Biotechnologies Inc.) to detect O-GlcNAcylated residues in peptide of AMFR.

Transmission electron microscopy

NRK cells were grown in 35 mm dishes precoated with fibronectin (10 µg/ml), and infected with VSV-GFP at an MOI of 0.2. At 8 hpi. The cells were prefixed at room temperature for 5 min using a 1:1 ratio of growth medium to 2.5% glutaraldehyde. Cells were further fixed with 2.5% glutaraldehyde in PB buffer for 2 h at room temperature, washed three times with PBS and dehydrated with a graded series of ethanol (50%, 70%, 90%, 95%, and 100%) for 8 min each. Samples were infiltrated with and embedded in SPON12 resin. After polymerizing for 48 h at 60 °C, 70-nm-thick ultrathin sections were cut using a diamond knife, and then picked up with Formvar-coated copper grids (100 mesh). The sections were double-stained with uranyl acetate and lead citrate. After air drying, samples were examined with a Hitachi H-7000FA transmission electron microscopy at 80 kV.

ER fractionation

Cells were collected in cold PBS and centrifuged at 600 × *g* for 5 min at 4 °C, removed the supernatant and resuspended the cells in 1 ml buffer E (20 mM HEPES, 250 mM sucrose, 1 mM EDTA, pH 7.4, 1 mM PMSF) and homogenized on ice by ultrasonic. The homogenates were centrifuged at 1000 × *g* for 10 min at 4 °C, then collected the supernatant as cytosol. Two-thirds of the cytosol fraction was further centrifuged at 8000 × *g* for 20 min at 4 °C, then the supernatant was transferred to ultracentrifuge tube and ultracentrifuged at 100,000 × *g* for 1 h at 4 °C. The obtained pellet was collected as the ER fraction.

Isolation of migrasomes

Migrasome isolation was performed by iodixanol-sucrose density gradient centrifugation using a Lysosome Isolation Kit (Sigma-Aldrich, 233-140-8). Cells were seeded in 150 mm dishes precoated with fibronectin (10 µg/ml) at 50% confluence, followed by VSV-GFP infection (MOI = 0.2). At 8 hpi, growth medium was disposed of and cells were washed to remove other extracellular vesicles in the medium. Cells were digested with trypsin and collected in 50 ml tubes. All subsequent manipulations were performed at 4 °C. Cells and large debris were removed and supernatants were collected by centrifugation at 1000 × *g* for 10 min followed by 4000 × *g* for 20 min. Crude migrasomes were then collected as the pellet by centrifugation at 18,000 × *g* for 30 min. Migrasomes fractionation was performed by density gradient centrifugation, using 5–50% Optiprep as the density medium (Sigma-Aldrich, LYSISO1). First, a step gradient was built starting with 50% (500 µl), followed by 40% (500 µl), 35% (500 µl), 30% (500 µl), 25% (500 µl), 20% (500 µl), 15% (500 µl), 10% (500 µl), 5% (500 µl) and crude migrasomes (5%, 800 µl). The crude migrasome sample was prepared by first resuspending the pellet with 400 µl 1 × extraction buffer mixed with 400 µl 10% Optiprep. Second, the prepared gradient was centrifuged at 150,000 × *g* for 4 hh at 4 °C in an MLS-50 rotor (Beckman). Finally, samples were collected from top to bottom (500 µl per fraction). Each fraction was mixed with the same volume of PBS (500 µl) and centrifuged at 18,000 × *g* for 30 min to collect the pellet. The pellets were washed with PBS and centrifuged again at 18,000 × *g* for 30 min. Fractions were prepared for TEM, plaque assay, infecting cells and western blot analysis.

Proteinase K protection assay

The isolated migrasomes pellet from VSV-GFP-infected cells were resuspended in PBS buffer and incubated on ice with 10 µg/ml proteinase K in the presence or absence of 0.1% Triton ×-100 for 30 min on ice. The reaction was terminated by addition of 1 mM PMSF. Samples were then subjected to western blot and viral plaque.

Statistics and reproducibility

Data are expressed as mean ± standard deviation (SD). The significance of the variability between different groups was determined by two-way analyses of variance using GraphPad Prism software (v9.5.1). Error bars, mean ± SD of two or three independent experiments. Two-tailed Unpaired Student's *t*-test. A p value of <0.05 was considered statistically significant and a p value of > 0.05 was considered statistically non-significant (ns). P value as exact values were given.

Reporting summary

Further information on research design is available in the Nature Portfolio Reporting Summary linked to this article.

Data availability

All data generated or analyzed during this study are included in this article and its supplemental materials. Source data are provided with this paper.

Code availability

Code applied to the analyses in this study can be found on Glyco POST at: https://glycopost.glycosmos.org (ID: GPST000657).

References

1. Jiao, H. F. et al. Mitocytosis, a migrasome-mediated mitochondrial quality-control process. *Cell* **184**, 2896–2910.e13 (2021).
2. Ma, L. et al. Discovery of the migrasome, an organelle mediating release of cytoplasmic contents during cell migration. *Cell Res.* **25**, 24–38 (2015).
3. Zhu, M. L. et al. Lateral transfer of mRNA and protein by migrasomes modifies the recipient cells. *Cell Res.* **31**, 237–240 (2021).
4. Jiang, D. et al. Migrasomes provide regional cues for organ morphogenesis during zebrafish gastrulation. *Nat. Cell Biol.* **21**, 966–977 (2019).
5. Zhang, C. F. et al. Monocytes deposit migrasomes to promote embryonic angiogenesis. *Nat. Cell Biol.* **24**, 1726–1738 (2022).
6. Hu, M. Y. et al. Macrophage lineage cells-derived migrasomes activate complement-dependent blood-brain barrier damage in cerebral amyloid angiopathy mouse model. *Nat. Commun.* **14**, 19 (2023).
7. Schmidt-Pogoda, A. et al. Dietary salt promotes ischemic brain injury and is associated with parenchymal migrasome formation. *PLoS ONE* **13**, 17 (2018).
8. Wu, L. J. et al. TSPAN4-positive migrasome derived from retinal pigmented epithelium cells contributes to the development of proliferative vitreoretinopathy. *J. Nanobiotechnol.* **20**, 17 (2022).
9. Liu, Y. L., Zhu, Z. Y., Li, Y. C., Yang, M. S. & Hu, Q. X. Migrasomes released by HSV-2-infected cells serve as a conveyance for virus spread. *Virol. Sin.* **38**, 643–645 (2023).
10. Lv, L. & Zhang, L. L. Identification of poxvirus inside migrasomes suggests a novel mode of mpox virus spread. *J. Infect.* **87**, 160–162 (2023).
11. Zhang, N., Gao, S. & Zhang, L. L. Chikungunya virus nsP1 induces migrasome formation. *J. Infect.* **85**, E158–E161 (2022).

12. Zhao, W. B., Tang, X. C. & Zhang, L. L. Virus-containing migrasomes enable poxviruses to evade tecovirimat/ST-246 treatment. *J. Infect.* **88**, 203–205 (2024).
13. Huang, Y. & Yu, L. Seeing is believing: observation of migrasomes. *Biophys. Rep.* **10**, 67–81 (2024).
14. Rubinstein, E. The complexity of tetraspanins. *Biochem. Soc. Trans.* **39**, 501–505 (2011).
15. Charrin, S. et al. Lateral organization of membrane proteins: tetraspanins spin their web. *Biochem. J.* **420**, 133–154 (2009).
16. Huang, Y. W. et al. Migrasome formation is mediated by assembly of micron-scale tetraspanin macrodomains. *Nat. Cell Biol.* **21**, 1301–1301 (2019).
17. Liang, H. S. et al. The formation of migrasomes is initiated by the assembly of sphingomyelin synthase 2 foci at the leading edge of migrating cells. *Nat. Cell Biol.* **25**, 1173 (2023).
18. Stiles, K. M. & Kielian, M. Role of TSPAN9 in alphavirus entry and early endosomes. *J. Virol.* **90**, 4289–4297 (2016).
19. Ooi, Y. S., Stiles, K. M., Liu, C. Y., Taylor, G. M. & Kielian, M. Genome-wide RNAi screen identifies novel host proteins required for alphavirus entry. *PLoS Pathog.* **9**, e1003835 (2013).
20. Malla, R. & Kamal, M. A. Tetraspanin-enriched Microdomain Containing CD151, CD9, and TSPAN 8 - Potential Mediators of Entry and Exit Mechanisms in Respiratory Viruses Including SARS-CoV-2. *Curr. Pharm. Des.* **28**, 3649–3657 (2022).
21. Hysenaj, L. et al. SARS-CoV-2 infection of airway organoids reveals conserved use of tetraspanin-8 by ancestral, delta, and omicron variants. *Stem. Cell Reports* **18**, 636–653 (2023).
22. Mekky, R. Y. et al. Mir-194 is a hepatocyte gate keeper hindering HCV entry through targeting CD81 receptor. *J. Infect.* **70**, 78–87 (2015).
23. Ashfaq, U. A., Qasim, M., Yousaf, M. Z., Awan, M. T. & Jahan, S. Inhibition of HCV 3a genotype entry through host CD81 and HCV E2 antibodies. *J. Transl. Med.* **9**, 194 (2011).
24. Hoshino, H. Cellular factors involved in HTLV-1 entry and pathogenicit. *Front. Microbiol.* **3**, 222 (2012).
25. Pique, C. et al. Interaction of CD82 tetraspanin proteins with HTLV-1 envelope glycoproteins inhibits cell-to-cell fusion and virus transmission. *Virology* **276**, 455–465 (2000).
26. Hart, G. W., Slawson, C., Ramirez-Correa, G. & Lagerlof, O. Cross talk between O-GlcNAcylation and phosphorylation: roles in signaling, transcription, and chronic disease. *Annu Rev Biochem.* **80**, 825–858 (2011).
27. Yang, X. Y. & Qian, K. V. Protein *O*-GlcNAcylation: emerging mechanisms and functions. *Nat. Rev. Mol. Cell Biol.* **18**, 452–465 (2017).
28. Ding, T. L. et al. The phosphatidylinositol (4,5)-bisphosphate-Rab35 axis regulates migrasome formation. *Cell Res.* **33**, 617–627 (2023).
29. Podbilewicz, B. Virus and cell fusion mechanisms. *Annu. Rev. Cell Dev. Biol.* **30**, 111–139 (2014).
30. Fang, S. Y. et al. The tumor autocrine motility factor receptor, gp78, is a ubiquitin protein ligase implicated in degradation from the endoplasmic reticulum. *Proc. Natl. Acad. Sci. USA.* **98**, 14422–14427 (2001).
31. Song, T. J. et al. DOT1L *O*-GlcNAcylation promotes its protein stability and MLL-fusion leukemia cell proliferation. *Cell Reports* **36**, 20 (2021).
32. Gupta, R. & Brunak, S. Prediction of glycosylation across the human proteome and the correlation to protein function. *Pac. Symp. Biocomput.* **7**, 310–322 (2002).
33. Wang, Q. et al. The E3 Ubiquitin Ligase AMFR and INSIG1 bridge the activation of TBK1 kinase by modifying the adaptor STING. *Immunity* **41**, 919–933 (2014).
34. Yu, S. B. & Yu, L. Migrasome biogenesis and functions. *Febs J* **289**, 7246–7254 (2022).
35. Dharan, R. et al. Transmembrane proteins tetraspanin 4 and CD9 sense membrane curvature. *Proc. Natl. Acad. Sci. USA.* **119**, 7 (2022).
36. Dharan, R. et al. Tetraspanin 4 stabilizes membrane swellings and facilitates their maturation into migrasomes. *Nat. Commun.* **14**, 9 (2023).
37. Huang, Y. W., Zhang, X., Wang, H. W. & Yu, L. Assembly of tetraspanin-enriched macrodomains contains membrane damage to facilitate repair. *Nat. Cell Biol.* **24**, 825–832 (2022).
38. Wang, D. J. & Yu, L. Migrasome biogenesis: when biochemistry meets biophysics on membranes. *Trends Biochem. Sci.* **49**, 829–840 (2024).
39. Shimizu, K. et al. The autocrine motility factor receptor gene encodes a novel type of seven transmembrane protein. *FEBS Lett.* **456**, 295–300 (1999).
40. Watanabe, H. et al. Purification of human tumor cell autocrine motility factor and molecular cloning of its receptor. *The Journal of Biological Chemistry* **266**, 13442–13448 (1991).
41. Zhang, H. H. et al. AMFR drives allergic asthma development by promoting alveolar macrophage-derived GM-CSF production. *J. Exp. Med.* **219**, 23 (2022).
42. Mookherjee, D. et al. RETREG1/FAM134B mediated autophagosomal degradation of AMFR/GP78 and OPA1-a dual organellar turnover mechanism. *Autophagy* **17**, 1729–1752 (2021).
43. Foronda, H. et al. Heteromeric clusters of ubiquitinated ER-shaping proteins drive ER-phagy. *Nature* **618**, 402–410 (2023).
44. Song, B. L., Sever, N. & DeBose-Boyd, R. A. Gp78, a membrane-anchored ubiquitin ligase, associates with Insig-1 and couples sterol-regulated ubiquitination to degradation of HMG CoA reductase. *Mol. Cell* **19**, 829–840 (2005).
45. Tewari, D. N., Biswas, A., Chakrabarti, A. K. & Dutta, S. AMFR promotes innate immunity activation and proteasomal degradation of HMGCR in response to influenza virus infection in A549 cells. *Virology* **587**, 14 (2023).
46. Jacobs, J. L., Zhu, J. Z., Sarkar, S. N. & Coyne, C. B. Regulation of mitochondrial antiviral signaling (MAVS) expression and signaling by the mitochondria-associated endoplasmic reticulum membrane (MAM) protein Gp78. *J. Biol. Chem.* **289**, 1604–1616 (2014).
47. Qian, G. et al. Glutamylation of an HIV-1 protein inhibits the immune response by hijacking STING. *Cell Reports* **42**, 21 (2023).

Acknowledgements

We thank professor Li Yu (Tsinghua University) for shCert, shCers5, shSgms2, sgRab35, sgTSPAN4, sgPIP5K1A, GFP tagged TSPAN4 and ITGA5, and L929 TSPAN4-mCherry cells, NRK cells and L929 ITGA5-GFP cells; professor Yuwei Huang (Xian Jiaotong University) for mCherry-TSPAN1, mCherry-TSPAN2, mCherry-TSPAN8, and mCherry-TSPAN9; professor Mingzhou Chen (Hubei University) for VSV-GFP and HSV-1; professor Yujie Ren (Wuhan Institute of Virology) and professor Junjie Zhang (Wuhan University) for HSV-1-UL17-Flag, HSV-1-UL5-Flag and HSV-1-ICP4-Flag; professor Lidong Sun (Huazhong University of Science and Technology) for Myc tagged OGA; professor Hong Zhang (Chinese Academy of Sciences) for GST tagged full length OGT; professor Yaxin Li (Guangzhou National Laboratory) for help with prediction of the structure of AMFR-TSPAN4 complex; Pei Zhang (Wuhan Institute of Virology) for TEM assistance. This work was supported by the National Natural Science Foundation of China (32422021, 32370809, U22A20337), the Major Project of Guangzhou National Laboratory (GZNL2024A01008), and project GZNL2024B01005, supported by Guangzhou National Laboratory and State Key Laboratory of Respiratory Disease, Guangzhou Medical University.

Author contributions

L.Y., J.L., and Y.H. performed most of experiments. X.Y. and W.Z. contributed with cloning, quantification, and repeating. Y.J. and Y.F. contributed with imaging and quantification. L.C. contributed with virus infection and plaque assay. B.D. conceived the project, designed the experiments, analyzed the data. B.D. and L.Y. wrote the manuscript. All authors discussed the results and commented on the manuscript.

Competing interests
The authors declare no competing interests.

Additional information
Supplementary information The online version contains supplementary material available at https://doi.org/10.1038/s41467-025-68220-3.

Correspondence and requests for materials should be addressed to Linling Cheng or Binbin Ding.

Peer review information *Nature Communications* thanks the anonymous, reviewer(s) for their contribution to the peer review of this work. A peer review file is available.

Reprints and permissions information is available at http://www.nature.com/reprints

Publisher's note Springer Nature remains neutral with regard to jurisdictional claims in published maps and institutional affiliations.

Open Access This article is licensed under a Creative Commons Attribution-NonCommercial-NoDerivatives 4.0 International License, which permits any non-commercial use, sharing, distribution and reproduction in any medium or format, as long as you give appropriate credit to the original author(s) and the source, provide a link to the Creative Commons licence, and indicate if you modified the licensed material. You do not have permission under this licence to share adapted material derived from this article or parts of it. The images or other third party material in this article are included in the article's Creative Commons licence, unless indicated otherwise in a credit line to the material. If material is not included in the article's Creative Commons licence and your intended use is not permitted by statutory regulation or exceeds the permitted use, you will need to obtain permission directly from the copyright holder. To view a copy of this licence, visit http://creativecommons.org/licenses/by-nc-nd/4.0/.

© The Author(s) 2026